C.E. SACLAY
DSM

SERVICE DE PHYSIQUE DES PARTICULES

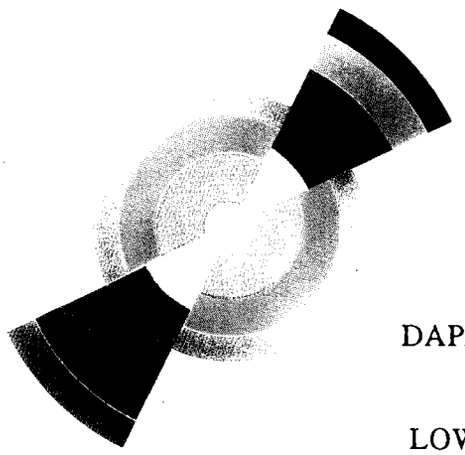

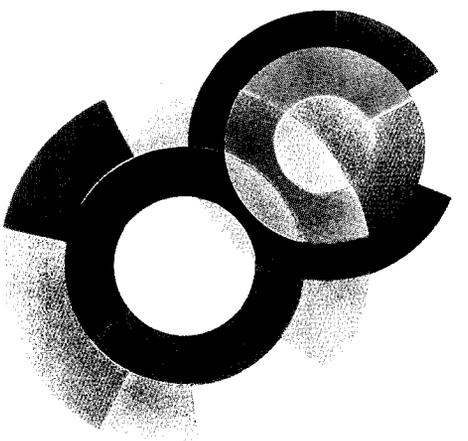

DAPNIA/SPP 94-35 November 1994

LOW X PHYSICS, DEEP INELASTIC SCATTERING AND STRUCTURE FUNCTIONS

J. FELTESSE

DAPNIA

Rapporteur talk at 24th International Conference on High Energy Physics, Glasgow, July 20-27 1994

Le DAPNIA (**D**épartement d'**A**strophysique, de physique des **P**articules, de physique **N**ucléaire et de l'**I**nstrumentation **A**ssociée) regroupe les activités du Service d'Astrophysique (SAp), du Département de Physique des Particules Elémentaires (DPhPE) et du Département de Physique Nucléaire (DPhN).

Adresse : DAPNIA, Bâtiment 141
CEA Saclay
F - 91191 Gif-sur-Yvette Cedex

Low x Physics, Deep Inelastic Scattering and Structure Functions

Joël Feltesse

CEA, DAPNIA/DSM/Service de Physique des Particules, CE-Saclay
F-91191 Gif-sur-Yvette Cedex, France

Rapporteur talk at 27th International Conference on High Energy Physics, Glasgow, July 20-27 1994

Low x Physics, Deep Inelastic Scattering and Structure Functions

Joël Feltesse

CEA, DAPNIA/DSM/Service de Physique des Particules, CE-Saclay
F-91191 Gif-sur-Yvette Cedex, France

Abstract

HERA experiments together with polarised fixed target lepton-nucleon scattering experiments and hadron-hadron interactions have provided this year a wealth of new results on the structure of the proton and on low x physics. Measurement of the W charge asymmetry in CDF at FNAL has provided new constraints on the d/u ratio in the proton. The Drell-Yan asymmetry $(\sigma_{pp}-\sigma_{pn})/(\sigma_{pp}+\sigma_{pn})$ measured by the NA51 experiment at CERN confirms that there are more $\bar{d}$ than $\bar{u}$ in the proton. New data on proton, deuteron and neuton polarized structure functions from the SLAC E143 and CERN SMC experiments are in good agreement. The naive Ellis-Jaffe sum rule is violated by at least two standard deviations and the Bjorken Sum rule is verified to within about 10%. The measured QCD corrections to the Bjorken Sum Rule using the low Q^2 data from E143 provide a new method to determine the QCD running coupling constant α_s. Combining fixed target data from E665 and FNAL and HERA results from H1 and ZEUS, the measurements of the proton structure function $F_2(x,Q^2)$ cover the very large kinematic range of $0.3 < Q^2 < 10^4$ GeV^2 and $2 \cdot 10^{-4} < x < 1$. The steep rise of the structure function F_2 with x decreasing is observed at x values below 10^{-1} and up to Q^2 values of about 1000 GeV^2. The interpretation of the F_2 behaviour at low x by the BFKL and GLAP mechanisms is discussed together with possible 'footprints' of the BFKL dynamics in the hadronic final states of deep inelastic scattering events at HERA. The properties of the deep inelastic scattering events at HERA with no energy in a large gap of rapidity close to the proton direction are reviewed. A signal from rapidity gap events in CDF and D0 experiments is presented.

1. Introduction

In the years 1991 and 1992 it was commonly believed that lepton nucleon deep inelastic scattering (DIS) on a fixed target, in particular the measurement of the structure of the nucleon, had reached a stable level of maturity, waiting for a renewal of the field with the advent of the first electron-proton collider HERA. Such a rejuvenation has indeed occurred with spectacular results at low x, where x is the fraction of momentum carried by the struck quark in lepton nucleon scattering. But fascinating results on the structure of the nucleon are still coming from deep inelastic fixed target experiments as well as from hadron-hadron interactions.

In this report, after a brief presentation of the latest data on quark densities in the nucleon, the impressive results on deep inelastic scattering off polarised targets are reviewed in more detail. The following part is then devoted to the measurement of the $F_2(x,Q^2)$ structure function where the most recent results from FNAL are combined with those from HERA to give access to the very large kinematic range in x and Q^2 : $0.3 < Q^2 < 10^4$ GeV^2 and $2 \cdot 10^{-4} < x < 1$. This is completed by a short discussion on low x phenomenology. In the last part an overview of the rapidity gap events in deep inelastic scattering is given together with their possible connection with the rapidity

gap events observed at FNAL.

2. Quark densities in the nucleon

2.1. W charge asymmetry

$W^+(W^-)$ bosons are produced in $\bar{p}p$ collisions primarily by the annihilation of $u(d)$ quarks from the proton and $\bar{d}(\bar{u})$ quarks from the antiproton. Because the u quarks carry more momentum on average than the d quarks the $W^+(W^-)$ tend to follow the direction of the incoming proton (antiproton). The W charge asymmetry is related to the d/u quark ratio in the proton [1]. What is actually measured is the lepton asymmetry

$$A(\eta) = \frac{d\sigma^+/d\eta - d\sigma^-/d\eta}{d\sigma^+/d\eta + d\sigma^-/d\eta} \qquad (1)$$

where $d\sigma^+(d\sigma^-)$ is the cross section for $W^+(W^-)$ decay leptons as a function of η the lepton rapidity. The asymmetry of W decays to electrons and muons measured by the CDF collaboration [2] is shown in figure 1. It is based on data recorded during the 1992-1993 run of the Tevatron collider. The asymmetry is sensitive to the ratio of d/u quark in the proton in the very high Q^2 ($\approx M_W^2$) and low x region ($0.007 < x < 0.24$). The measurement provides a new test of the parametrizations of the quark densities in the proton (see figure 1). The recent parametrizations of the CTEQ collaboration [3] which fit the most precise fixed target data predict a too large asymmetry in contrast to those of the Durham group [4, 5, 6]. which give a good description of the data.

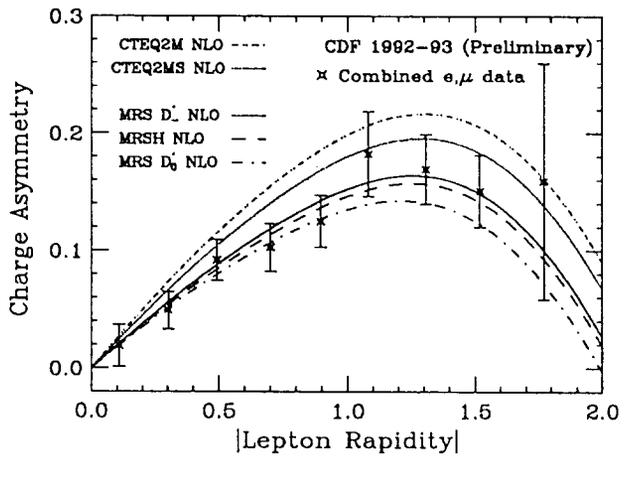

Figure 1. The charge asymmetry measured by CDF, compared with the latest parton distribution parametrizations. The asymmetry at negative η is combined with that at positive η assuming CP invariance. The systematic errors are included.

2.2. Gottfried Sum

At this conference, the NMC collaboration has presented a slighly updated value for the Gottfried sum at $Q^2 = 4$ GeV^2 [7]:

$$S_G = \int_0^1 (F_2^p - F_2^n)\frac{dx}{x} = 0.235 \pm 0.026. \qquad (2)$$

What is actually measured is the Gottfried sum for $x > 0.004$. The contribution to the unknown very low x region has been estimated assuming that $F_2^p - F_2^n$ has a smooth Regge-like behaviour ax^b from $x = 0.15$ down to $x = 0$. The new determination from NMC is based on a re-evaluation of the radiative correction using the most recent results for F_2^d and an improved understanding of the momentum calibration. The result is close to the previous published value $S_G = 0.240 \pm 0.016$ [8].
The data were not corrected for shadowing effects in deuterium, but if anything they should even reduce S_G by 15 %.

In the quark parton model (QPM) and assuming isospin invariance, which relates the parton distribution of the proton and neutron through the interchange $u \leftrightarrow d$, the Gottfried sum reads :

$$S_G = \frac{1}{3} + \frac{2}{3}\int_0^1 (\bar{u} - \bar{d})dx \qquad (3)$$

which is then equal to 1/3 for a $\bar{u} - \bar{d}$ flavour-symmetric sea (Gottfried Sum Rule). The NMC result indicates a clear violation of this sum rule and that the light-quark sea is flavour asymmetric. There are more $\bar{d}$ than $\bar{u}$ in the proton. This interpretation has however been questioned because the extrapolation to $x = 0$ is model dependent. It is possible, although a bit artificial, to build parametrizations of the valence quarks momentum distributions which describe the NMC data and yet satisfy the Gottfried sum rule [9].

2.3. Drell-Yan Asymmetry

Ellis and Stirling [10] have suggested the comparison of dilepton production by protons on proton and neutron targets (Drell-Yan process):

$$A_{DY} = \frac{\sigma_{pp} - \sigma_{pn}}{\sigma_{pp} + \sigma_{pn}} \qquad (4)$$

where σ^{pp} and σ^{pn} are the cross sections for dileptons produced in $p - p$ and $p - n$ collisions. At 90^0 in the centre of mass of the interaction and neglecting the sea-sea contributions the asymmetry becomes :

$$A_{DY} = \frac{(4u_V - d_V)(\bar{u} - \bar{d}) + (u_V - d_V)(4\bar{u} - \bar{d})}{(4u_V + d_V)(\bar{u} + \bar{d}) + (u_V + d_V)(4\bar{u} + \bar{d})} \qquad (5)$$

A_{DY} depends only on the up quark to down quark ratios for the valence and sea quark distributions. The NA51

collaboration has measured the Drell-Yan asymmetry at CERN using a primary beam of 450 GeV incident protons and targets of liquid hydogen and deuterium. Muons are detected in the NA10 spectrometer. Muon pairs with mass higher than 4.3 GeV^2 provide an asymmetry at the mean x value $< x >= 0.18$. In this x region the valence quark distributions are well known. For a light-quark flavour-symmetric sea A_{DY} is predicted to be positive $A_{DY} = 0.09$. The NA51 collaboration finds [11] :

$$A_{DY} = -0.09 \pm 0.02(stat) \pm 0.025(syst) \quad (6)$$

The ratio $\frac{\bar{u}}{\bar{d}}$ at $x = 0.18$ deduced from this measurement is :

$$\frac{\bar{u}}{\bar{d}} = 0.51 \pm 0.04(stat) \pm 0.05(syst) \quad (7)$$

This is another indication that the light quark sea is not flavour symmetric. The result is consistent with the NMC measurement but has necessitated a revision of the parametrization of the Durham group. A new set (MRSA) has been produced which describes the Drell-Yan and the W rapidity asymmetry measurements [12].

To conclude this section it is worth remembering that the analysis of dimuon events in neutrino scattering experiments has already shown that the nucleon strange quark content is suppressed with respect to the non-strange sea quarks by a factor [13] :

$$\kappa = \frac{\int_0^1 (xs + x\bar{s})dx}{\int_0^1 (x\bar{u} + x\bar{d})dx} = 0.477^{+0.063}_{-0.053} \quad (8)$$

The measurements from the Gottfried Sum Rule and from Drell-Yan asymmetry show that the light-quark sea is also flavour asymmetric. At moderate or large x the flavour composition of the proton is still mysterious.

3. Spin Structure Functions

Another method to gain insight into the structure of the nucleon is to measure the fraction of the nucleon spin carried by the quark spins or more generally to study the internal spin structure of the proton and the neutron. Polarised lepton-nucleon scattering experiments measure the asymmetry :

$$A_m(x, Q^2) = \frac{d\sigma^{\uparrow\uparrow}(x, Q^2) - d\sigma^{\uparrow\downarrow}(x, Q^2)}{d\sigma^{\uparrow\uparrow}(x, Q^2) + d\sigma^{\uparrow\downarrow}(x, Q^2)} \quad (9)$$

where $d\sigma\uparrow\uparrow$ ($d\sigma\uparrow\downarrow$) is the cross section when the incoming lepton and the nucleon spin are parallel (antiparallel) to each other. For a proton target the measured asymmetry A_m^p is related to the virtual-photon proton asymmetries A_1 and A_2 by

$$A_1^p = \frac{A_m^p}{D} - \eta A_2^p. \quad (10)$$

D, the depolarisation factor, depends on $R(x, Q^2)$, where R is the cross section ratio of longitudinally and transversely polarised photons, $R = \sigma_L/\sigma_T$. η is a kinematic factor which depends on x and Q^2. The asymmetry A_2^p arises from the interference between transverse and longitudinal virtual photon polarisations and is constrained by the positivity limit $|A_2^p| \leq \sqrt{R}$. A_2 is expected to give a very small contribution. The A_1 asymmetry is related to the polarised and unpolarised structure functions $g_1(x, Q^2)$ and $F_1(x, Q^2)$:

$$g_1(x, Q^2) = F_1(x, Q^2)[A_1(x, Q^2) + \gamma A_2(x, Q^2)] \quad (11)$$

where γ is a kinematic factor given by $\gamma = 2M_p x/\sqrt{Q^2}$. In the quark parton model the structure functions F_1 and g_1 have a simple interpretation :

$$g_1(x) = \frac{1}{2}\sum_i e_i^2[q_i^{\uparrow}(x) + \bar{q}_i^{\uparrow}(x) - q_i^{\downarrow}(x) - \bar{q}_i^{\downarrow}] \quad (12)$$

$$F_1(x) = \frac{1}{2}\sum_i e_i^2[q_i^{\uparrow}(x) + \bar{q}_i^{\uparrow}(x) + q_i^{\downarrow}(x) + \bar{q}_i^{\downarrow}] \quad (13)$$

where the sum is over the different quark and antiquark flavours, e_i is the quark electric charge and $q_i^{\uparrow}$ ($q_i^{\downarrow}$) is the density of quarks with spin parallel (antiparallel) to the nucleon spin. In a static picture of proton and neutron consisting of pure valence quarks the proton asymmetry A_1^p is 5/9 and the neutron asymmetry is 0. As is the case for the structure function F_1, perturbative QCD cannot predict the absolute value of g_1. However very important sum rules have been derived.

3.1. The Bjorken Sum Rule

The only rigorous sum rule for polarized deep-inelastic scattering is the Bjorken Sum Rule for the differences of the first moments of g_1^p and g_1^n [14] :

$$\Gamma_1^p - \Gamma_1^n = \int_0^1 (g_1^p - g_1^n)dx = \frac{1}{6}\left|\frac{g_A}{g_V}\right|\left[1 - \Delta_{QCD}^{NS}\right] \quad (14)$$

where g_A and g_V are the axial-vector and vector weak coupling constants of nuclear beta decay, yielding an asymptotic value of 0.21. The Bjorken Sum Rule is an inescapable prediction of QCD [15]. Δ_{QCD}^{NS}, the perturbative QCD correction, has been calculated in the $\bar{MS}$ prescription for $N_f = 3$ flavours, up to the third order in α_s [16], and an estimate has been made of the fourth order coefficient [17] :

$$\Delta_{QCD}^{NS} = \left[\left(\frac{\alpha_s(Q^2)}{\pi}\right) + 3.5833\left(\frac{\alpha_s(Q^2)}{\pi}\right)^2 + 20.2153\left(\frac{\alpha_s(Q^2)}{\pi}\right)^3 + 130\left(\frac{\alpha_s(Q^2)}{\pi}\right)^4 + \cdots\right] \quad (15)$$

3.2. The Ellis Jaffe Sum Rule

Separate sum rules for the polarised proton and neutron structure functions have also been proposed [18]. In the quark parton model (Equation (12)) the sum rules can be written as

$$\int_0^1 g_1^p dx = \frac{1}{18}(4\Delta u + \Delta d + \Delta s) \quad (16)$$

$$\int_0^1 g_1^n dx = \frac{1}{18}(4\Delta d + \Delta u + \Delta s) \quad (17)$$

where for example Δu is the net polarisation carried by the quarks and antiquarks u and $\bar{u}$

$$\Delta u = \int_0^1 (u^{\uparrow}(x) + \bar{u}^{\uparrow}(x) - u^{\downarrow}(x) + \bar{u}^{\downarrow}(x))dx \quad (18)$$

Assuming that strange quarks and antiquarks in a polarised nucleon have no net polarisation, Ellis and Jaffe predict that :

$$\Gamma_1^p = \int_0^1 g_1^p dx \approx 0.17 \quad (19)$$

$$\Gamma_1^n = \int_0^1 g_1^n dx \approx -0.02 \quad (20)$$

Perturbative QCD corrections to the Ellis-Jaffe sum rules have also been calculated. The sums have to be decomposed into singlet and non-singlet terms :

$$\int_0^1 g_1^p dx = \frac{1}{18}\left[(2\Delta u + \Delta d - \Delta s)(1 - \Delta_{QCD}^{NS}) + 2(\Delta u + \Delta d + \Delta s)(1 - \Delta_{QCD}^{S})\right] \quad (21)$$

Δ_{QCD}^{NS}, the corrections to the non-singlet terms, are those of the Bjorken Sum Rule. Δ_{QCD}^{S}, the corrections to the singlet terms, have been calculated up to second order in α_s [19] and an estimate has been made of the third order coefficient [20].

$$\Delta_{QCD}^{S} = \left[\left(\frac{\alpha_s(Q^2)}{\pi}\right) + 1.0959\left(\frac{\alpha_s(Q^2)}{\pi}\right)^2 + 6\left(\frac{\alpha_s(Q^2)}{\pi}\right)^3 + \cdots\right] \quad (22)$$

3.3. The new data

Following the pioneering experiments of SLAC (E80 and E130) [21, 22] and CERN (EMC [25]) new data have been presented at this conference from experiments on both sides of the Atlantic.

3.3.1. SMC The SMC collaboration at CERN has presented [23] new results on the structure function g_1^p (figure 2) from deep inelastic scattering of a 190 GeV polarised muon beam off a polarised target of butanol. The kinematic range is $0.003 < x < 0.7$ and $1 < Q^2 < 60$ GeV^2. To evaluate the integral Γ_1^p, it has been assumed that g_1^p is constant at $x < 0.003$ and that the asymmetry A_1^p is constant at $x > 0.7$. The low x ($x < 0.003$) contribution to the integral amounts to 0.004 ± 0.004. The high x ($x > 0.007$) contribution amounts to 0.0015 ± 0.0007. In the asymmetry measurement each bin of x corresponds to a different Q^2 value. To get the Γ_1^p at a fixed Q^2 value, $Q_0^2 = 10$ GeV^2, g_1^p was recalculated using Equation (11) neglecting A_2 and assuming the ratio g_1/F_1 to be independent of Q^2. The result is :

$$\Gamma_p^1(10\ \mathrm{GeV}^2) = 0.136 \pm 0.011(stat.) \pm 0.011(syst.). \quad (23)$$

The main systematic errors are the uncertainty on the beam polarization, the uncertainty on F_1, the extrapolation at low x and the target polarization.

The Ellis-Jaffe sum rule of the proton predicts a value of 0.176 ± 0.006 after QCD corrections. The SMC measurement is two standard deviation below this value.

The SMC collaboration has also presented the first result of the spin asymmetry A_2^p in the scattering of 100 GeV longitudinally-polarized muons off a transversely polarized butanol target. The asymmetry is found to be compatible with zero (figure 3), well below the positivity limit $\sqrt{R}$ evaluated from the SLAC parametrization [24]. This confirms that the contribution of the A_2 term in extracting the g_1^p structure function (Equation (11)) is indeed negligible.

3.3.2. SLAC E143 The E143 SLAC collaboration has reported new preliminary results on the structure functions g_1^p, g_1^d and g_1^n. The data were taken with polarized electron beams of 29.1 GeV energy scattering off targets of ammonia granules of $^{15}NH_3$ and $^{15}ND_3$. The results cover the kinematic range $0.029 < x < 0.8$ and $1.3 < Q^2 < 10$ GeV^2. The asymmetry (g_1^p/F_1^p) measured by E143 at $< Q^2 >= 3$ GeV^2 and SMC at $< Q^2 >= 10$ GeV^2 are shown in figure 2 together with the old SLAC data. There is excellent agreement between all the measurements obtained with very different techniques and at different Q^2 confirming that the ratio g_1/F_1 is independent of Q^2 in the present kinematic range or, in other words, that the structure functions g_1 and F_1 have the same Q^2 dependence.

To extrapolate to $x = 0$, the E143 collaboration has observed that all data from SMC and EMC at $x < 0.1$ can be fitted by a constant value of $g_1^p = 0.28$ at $x < 0.1$. Using this constant the low x ($x < 0.029$) contribution

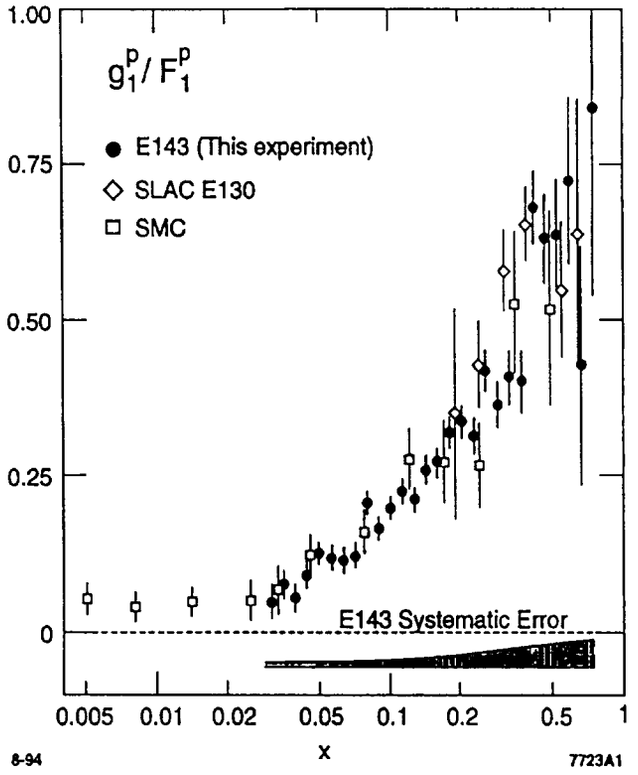

Figure 2. The ratio of the spin-dependent to the spin independent proton structure functions $g_1^p(x)/F_1^p(x)$ as a function of x. Only statistical errors are shown with the data points. The size of the systematic errors for the E143 points is indicated by the shaded area.

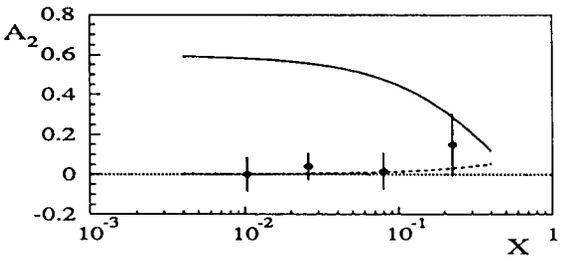

Figure 3. The asymmetry A_2 as a function of x. The data points are from SMC. The solid line shows $\sqrt{R}$ from the SLAC parametrization [24].

to the integral Γ_1^p amounts to 0.007 ± 0.005. The constant value of g_1^p is 4 times smaller than the mean value assumed by SMC at $x < 0.003$. However within the large quoted errors the extrapolations to $x = 0$ of SMC and E143 are still compatible.
The extrapolation to $x = 1$ gives a very small contribution to the integral : 0.002 ± 0.001, very close to the SMC estimate. The total integral at $Q_0^2 = 3$ GeV^2 is :

$$\Gamma_1^p(3\ \mathrm{GeV}^2) = 0.129 \pm 0.004(stat.) \pm 0.010(syst.). \quad (24)$$

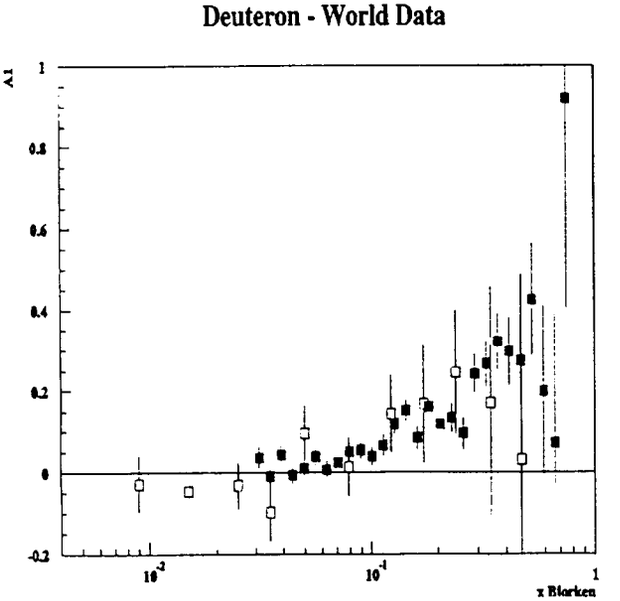

Figure 4. The virtual-photon deuteron cross section asymmmetry A_1^d as a function of x. The solid points are the preliminary data of from E143. The open points come from SMC.

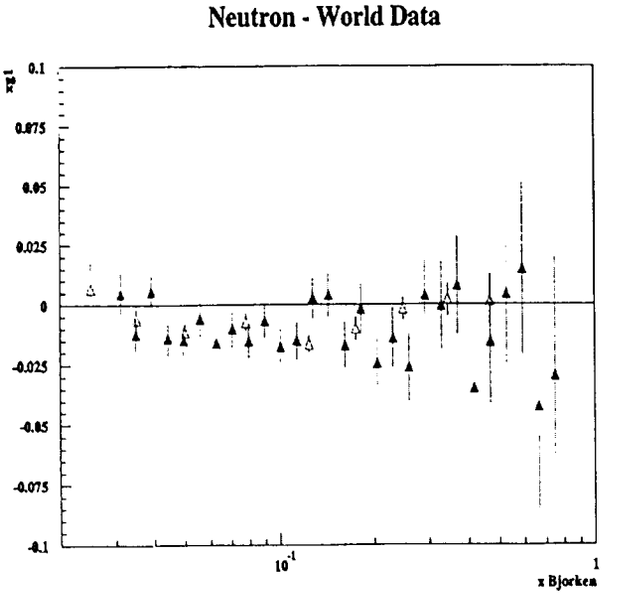

Figure 5. The spin-dependent structure function $xg_1^n(x)$ as a function of x. The solid points are the preliminary data of from E143. The open points come from E142.

The statistical error of E143 is significantly smaller than that of SMC but the systematic errors are almost identical. The quoted values of the two collaborations on the first moment of the structure function g_1^p are in good agreement although they were obtained at different Q^2 and with somewhat different assumptions to extrapolate to $x = 0$. The two new measurements agree also with the original EMC value of $0.123 \pm 0.013 \pm 0.015$. The E143 determination is well below the Ellis-Jaffe sum rule prediction of 0.160 ± 0.003 at $Q_0^2 = 3$ GeV^2 (see Table 1).

The E143 collaboration has also reported a new determination of the deuteron structure function with much smaller error than the previous determination of SMC [27]. Within the large errors of SMC, there is no discrepancy between the two experiments (figure 4). This yields a new determination of the first moment of the deuteron structure function at $Q_0^2 = 3$ GeV^2:

$$\Gamma_1^d(3 \text{ GeV}^2) = 0.044 \pm 0.003(stat.) \pm 0.004(syst.), \quad (25)$$

a value well below the Ellis-Jaffe prediction of 0.068 ± 0.004.

A very preliminary estimate of the neutron asymmetry has also been given (figure 5). The results are in agreement with those of E142 [28]. The estimate of Γ_1^n is :

$$\Gamma_1^n(3\ GeV^2) = -0.033 \pm 0.008(stat.) \pm 0.013(syst.). \quad (26)$$

3.4. Proton spin fraction carried by quarks

All data on the first moment of the polarized structure functions for the proton, neutron and deuteron are collected in Tables 1,2 and 3. The results for the proton and deuteron show a clear violation of the Ellis-Jaffe sum rule by at least two standard deviations, in contrast to the neutron results which do not indicate any deviation from the Ellis-Jaffe sum rule. This apparent contradiction between neutron and proton results disappears when higher order QCD corrections are applied and allowance is made for higher twist corrections [29, 30, 31, 32].

In a recent fit of all available data, except the very preliminary results of E143 on neutron, Ellis and Karliner have extracted $\Delta\Sigma(= \Delta u + \Delta d + \Delta s)$ and Δs. After applying QCD corrections up to at least third order in α_s neutron and proton results do agree within errors (figure 6). It is striking that the QCD corrections act differently on the first moment of the structure function g_1 for proton and neutron. The fit yields an average value for the proton spin fraction carried by the quarks :

$$\Sigma = 0.33 \pm 0.04. \quad (27)$$

The violation of the Ellis-Jaffe Sum Rule for the proton (figure 7) can be interpreted to be due to a non zero net spin carried by the strange quarks :

$$\Delta s = -0.10 \pm 0.04 \quad (28)$$

3.5. Extraction of $\alpha_s(Q^2)$

To check the Bjorken Sum rule the SMC collaboration has compiled all available data on proton, deuteron and neutron in April 1994, i.e. not including data from E143. All measurements of the structure functions g_1 have been re-evaluated at $Q^2 = 5$ GeV^2 assuming that the asymmetry $A_1(x, Q^2)$ is independent of Q^2. The measured sum is :

$$\Gamma_1^p - \Gamma_1^n = 0.163 \pm 0.017. \quad (29)$$

which agrees within 12% with the theoretical prediction of :

$$\Gamma_1^p - \Gamma_1^n = 0.185 \pm 0.004. \quad (30)$$

The prediction includes higher perturbative QCD corrections up to third order in α_s.

In a different approach, Ellis and Karliner have assumed that the Bjorken Sum Rule is valid to extract from the data an estimate of the QCD correction, Δ_{NS} (Equation (14)), and then, from the expression for these corrections up to fourth order (Equation (15)), have inferred a value of α_s . The method has been applied to the very recent data on proton and neutron of the E143 experiment, yielding an estimate of α_s at a mean Q^2 value of 2.5 GeV^2 [33]:

$$\alpha_s(2.5 \text{ GeV}^2)|_{MS,N_f=3} = 0.375^{+0.062}_{-0.081} \quad (31)$$

which corresponds to :

$$\alpha_s(M_Z^2)|_{MS,N_f=5} = 0.122^{+0.005}_{-0.009} \quad (32)$$

It is obviously questionable to neglect higher-twist effects at so small a value of Q^2. Taking into account a rough estimate of the higher-twist effect

$$\delta_{HT} = \frac{(-0.02 \pm 0.01) \text{ GeV}^2}{Q^2} \quad (33)$$

Ellis and Karliner find:

$$\alpha_s(M_Z^2)|_{MS,N_f=5} = 0.118^{+0.007}_{-0.014} \quad (34)$$

a value still not competitive with the best determinations but in good agreement with the world average [34]. This agreement shows that not only the Bjorken Sum Rule but also the corrections to the Sum Rule have been verified by the measurements. One may hope that in the future, with an improved precision of about a factor two in the data and a better control of the higher-twist corrections, the α_s determination from the polarized structure functions could become very competitive.

Proton Experiments	Beam	x range	$< Q^2 >$	$\int_0^1 g_1^p(x,Q^2)dx$ measured	Ellis-Jaffe prediction
E80 (1976)	e	0.1-0.5	2.		
E130 (1983)	e	0.2-0.6	4.	0.17 ± 0.05	
EMC (1988)	μ	0.015-0.7	10.	$0.123 \pm 0.013 \pm 0.019$	0.176 ± 0.006
SMC (1994)	μ	0.003-0.7	10.	$0.136 \pm 0.011 \pm 0.011$	0.176 ± 0.006
E143 (1994)	e	0.03-0.6	3.	$0.129 \pm 0.004 \pm 0.010$	0.160 ± 0.003

Table 1. Measurements of Γ_1^p compared with Ellis-Jaffe predictions after QCD corrections.

Deuteron Experiments	Beam	x range	$< Q^2 >$	$2\int_0^1 g_1^d(x,Q^2)dx$ measured	Ellis-Jaffe prediction
SMC (1993)	μ	0.006-0.6	4.6	$0.049 \pm 0.044 \pm 0.032$	0.187 ± 0.010
E143 (1994)	e	0.03-0.8	3.	$0.088 \pm 0.006 \pm 0.008$	0.136 ± 0.008

Table 2. Measurements of Γ_1^d compared with Ellis-Jaffe predictions after QCD corrections. SMC data have been corrected to get $\int_0^1 (g_1^p(x,Q^2) + g_1^n(x,Q^2))dx$.

Neutron Experiments	Beam	x range	$< Q^2 >$	$\int_0^1 g_1^n(x,Q^2)dx$ measured	Ellis-Jaffe prediction
E142 (1993)	e	0.03-0.6	2.	$-0.022 \pm 0.007 \pm 0.009$	-0.021 ± 0.018
E143 (1994)	e	0.03-0.8	3.	$-0.033 \pm 0.008 \pm 0.013$	

Table 3. Measurements of Γ_1^n compared with Ellis-Jaffe predictions after QCD corrections.

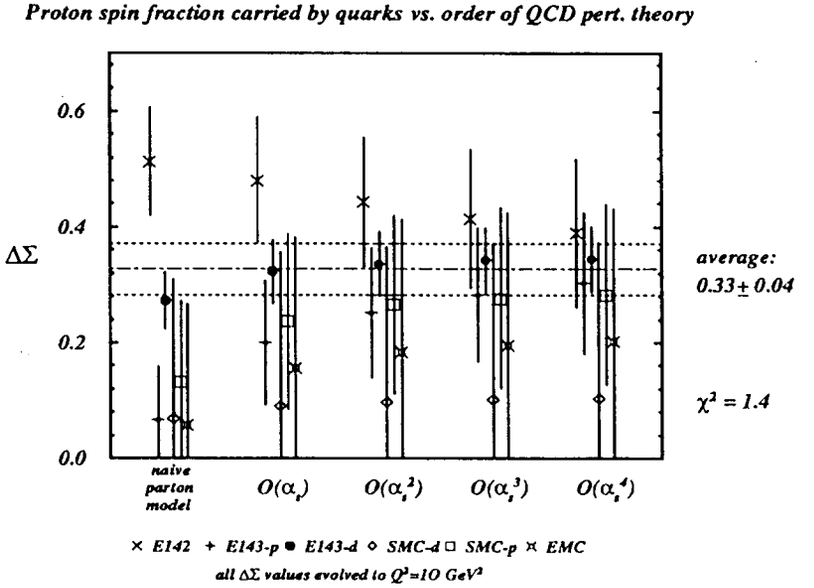

Figure 6. The values of $\Delta\Sigma(Q^2 = 10\ \mathrm{GeV}^2)$ plotted as functions of the increasing order of QCD perturbation theory used in extracting $\Delta\Sigma$ from the data.

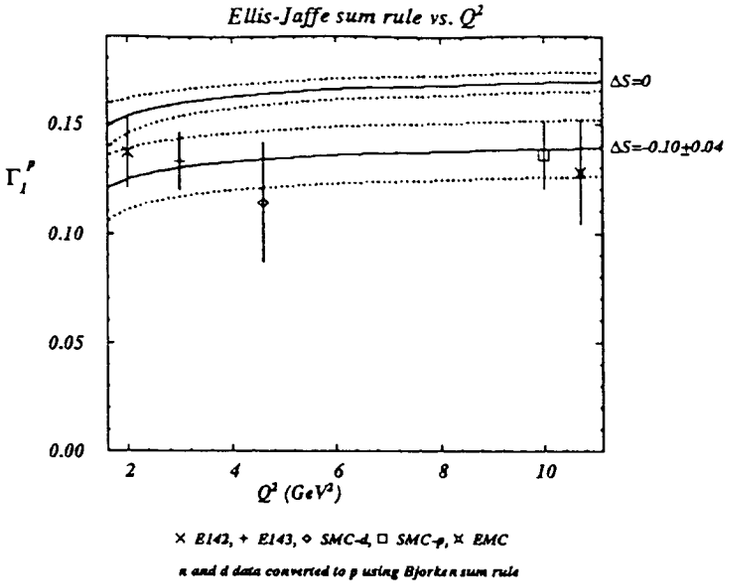

Figure 7. The integral Γ_1^p as a function of Q^2. The data come from EMC, SMC and E143 on protons, together with those inferred from E142 on neutrons and SMC on deuterons using the Bjorken Sum rule. The upper continuous curve shows the value if $\Delta s = 0$, together with an error band plotted as dotted curves. The lower curve shows the prediction if $\Delta s = -0.10 \pm 0.04$.

3.6. Low x extrapolations

The small-x behaviour of $g_1^{p,n}$ has recently been discussed. A contribution from the exchange of two non-perturbative gluons should generate a $|\log \frac{1}{x}|$ rise [35] with decreasing x rather than the flat or decreasing behaviour assumed by the experiments. An even stronger rise in $\frac{1}{x \log^2 x}$ seems not to be excluded by the theory [36]. The data of SMC on g_1^p may indicate some rise at very low x (figure 8) which is not yet statistically significant. Such an effect would cause Γ_p and Γ_n to increase, eventually approaching the Ellis-Jaffe predictions, but would cancel out in the difference. Any anticipated mechanism to generate a rise of g_1^p at low x should generate a similar rise of g_1^n [36]. A striking feature is that, as g_1^n is negative at $x \approx 0.05$, g_1^n would become positive at very low value of x.

Such a 'non-standard' rise of the structure functions g_1 at low x needs stronger experimental evidence and more solid theoretical justifications. It may be linked to the rise of the F_2 structure function at low x and would be definitely very interesting to observe.

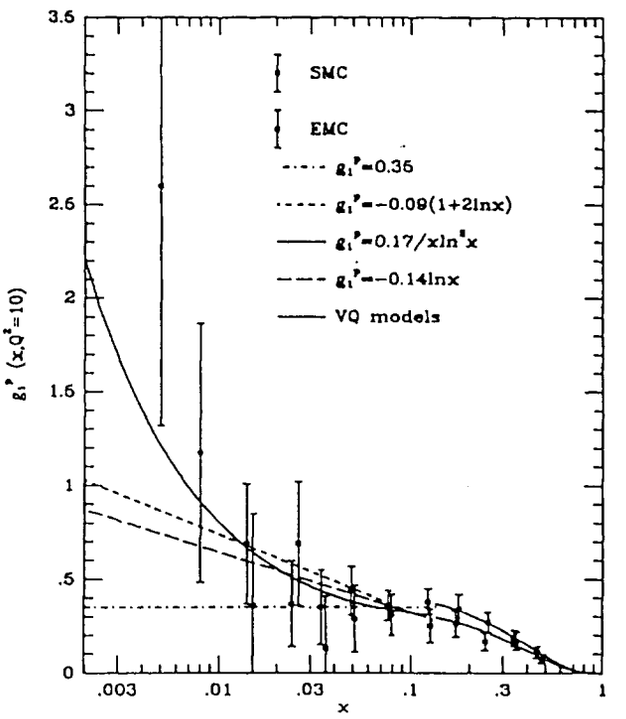

Figure 8. The structure function $g_1^p(x)$ at $Q^2 = 10$ GeV^2. Data from EMC and SMC are compared to various ansätze on the behaviour of g_1^p at very low x.

3.7. Future prospects

The field of polarized structure functions is of growing interest. Many new results are expected in the next years.

- At CERN, the SMC collaboration is recording new deuteron data in 1994 and should get more precise data in 1995 aiming for statistical errors of ± 0.008 on Γ_1^p.
- At SLAC two new experiments are planned with the new 50 GeV electron beam. E154 should run in late 1995 with an helium target to get the structure function g_1^n with twice the precision and at lower x than the previous SLAC experiments. The E155 experiment should run later with ammonia granules to get the structure functions g_1^p and g_1^n with improved statistical precision.
- At DESY, the HERMES collaboration should start to collect data in 1995. The electron beam from HERA collides with an ultra-pure polarized gas target. The HERMES experiment is specially designed to tag outgoing hadronic particles to measure asymmetries of semi-inclusive charged hadron cross sections, for example the positive hadron asymmetry measured with an hydrogen target

$$A_p^+ = \frac{(\sigma_{p\uparrow\downarrow}^+ - \sigma_{p\uparrow\uparrow}^+)}{(\sigma_{p\uparrow\downarrow}^+ + \sigma_{p\uparrow\uparrow}^+)} \qquad (35)$$

and similar asymmetries for negative hadrons and a neutron target. The asymmetries provide direct access to the fraction of the spin of the proton carried by valence quarks, strange and non-strange sea quarks. A first measurement of this asymmetry has been presented at this conference by the SMC collaboration [37]. The measured net spins carried by u_v and d_v valence quarks are shown in figure 9 together with the first parametrization of the spin structure function [38]. At $x \approx 0.3$, Δu_v and Δd_v are clearly positive and negative respectively. The method is very promising. The errors are expected to be an order of magnitude smaller in the HERMES experiment.

4. The Proton Structure Function $F_2(x, Q^2)$.

The kinematics of the inclusive lepton-nucleon deep inelastic scattering process $l\,p \rightarrow l\,X$ at centre of mass energy $\sqrt{s}$ is determined by two independent Lorentz-invariant variables, conventionally chosen to be two out of x, Q^2, the variables that we have used in the previous sections, and y, the fractional energy transfer to the photon in the nucleon rest frame. The Born cross section for DIS of a charged lepton off a proton is given in terms of structure functions as :

$$\frac{d^2\sigma(l^\pm)}{dxdQ^2} = \frac{2\pi\alpha^2}{Q^4 x}\left[\left(2\,(1-y) + \frac{y^2}{1+R}\right)F_2(x,Q^2) \mp \left(2y - \frac{y^2}{2}\right)xF_3(x,Q^2)\right] \qquad (36)$$

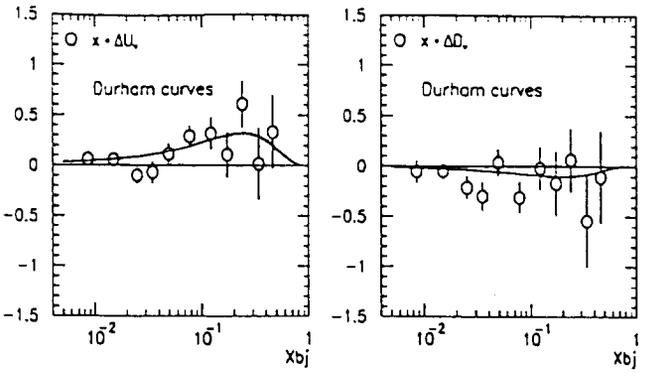

Figure 9. Polarised spin distributions of valence quarks measured from semi-inclusive cross section asymmetries by the SMC collaboration. The curves are parametrizations of the Durham group [38]

where R is the cross section ratio for longitudinally and transversely polarised photons, $R = \sigma_L/\sigma_T$. The contribution from R is negligible except at large y where assumptions have to be made until it can be measured. In the highest Q^2 range accessed by the present data ($Q^2 \approx 2000$ GeV^2) the contribution of the structure function xF_3 is still a small correction.

New results on the proton structure function $F_2(x, Q^2)$ have been presented at this conference from the FNAL muon scattering E665 experiment [39] and from the HERA experiments H1 [40] and ZEUS [41]. We can see (figure 10) that the x, Q^2 bins of the H1 data almost close the kinematical gap between the fixed target data of E665 and the HERA results. Together with the well established results on fixed targets from the BCDMS [42], NMC [43] and SLAC [44] experiments the (x, Q^2) region of the new data extends to : $0.3 < Q^2 < 10^4$ GeV^2 and $2 \cdot 10^{-4} < x < 1$.

4.1. E665

This year the preliminary results of the E665 collaboration on the structure function $F_2(x, Q^2)$ have been presented for the first time. The data were taken in 1991 in the 400−550 GeV muon beam at FNAL. The integrated luminosity on a hydrogen target is 0.7 pb^{-1}. The kinematic range starts at $Q^2 = 0.1$ GeV^2 and $x = 8\ 10^{-4}$. The Q^2 behaviour will be discussed together with the HERA data in the next section. The results as a function of x are shown in figure 11. For all Q^2 bins the data are remarkably flat in x. The systematic errors have not yet been included. The current systematic error is around 20% and is dominated by uncertainties on the scattered muon reconstruction. There is hope that the final error will be twice as small. There is also an additional unknown error due to the assumptions for R. The E665 experiment has used the parametrization of R from the SLAC data measured at much larger x val-

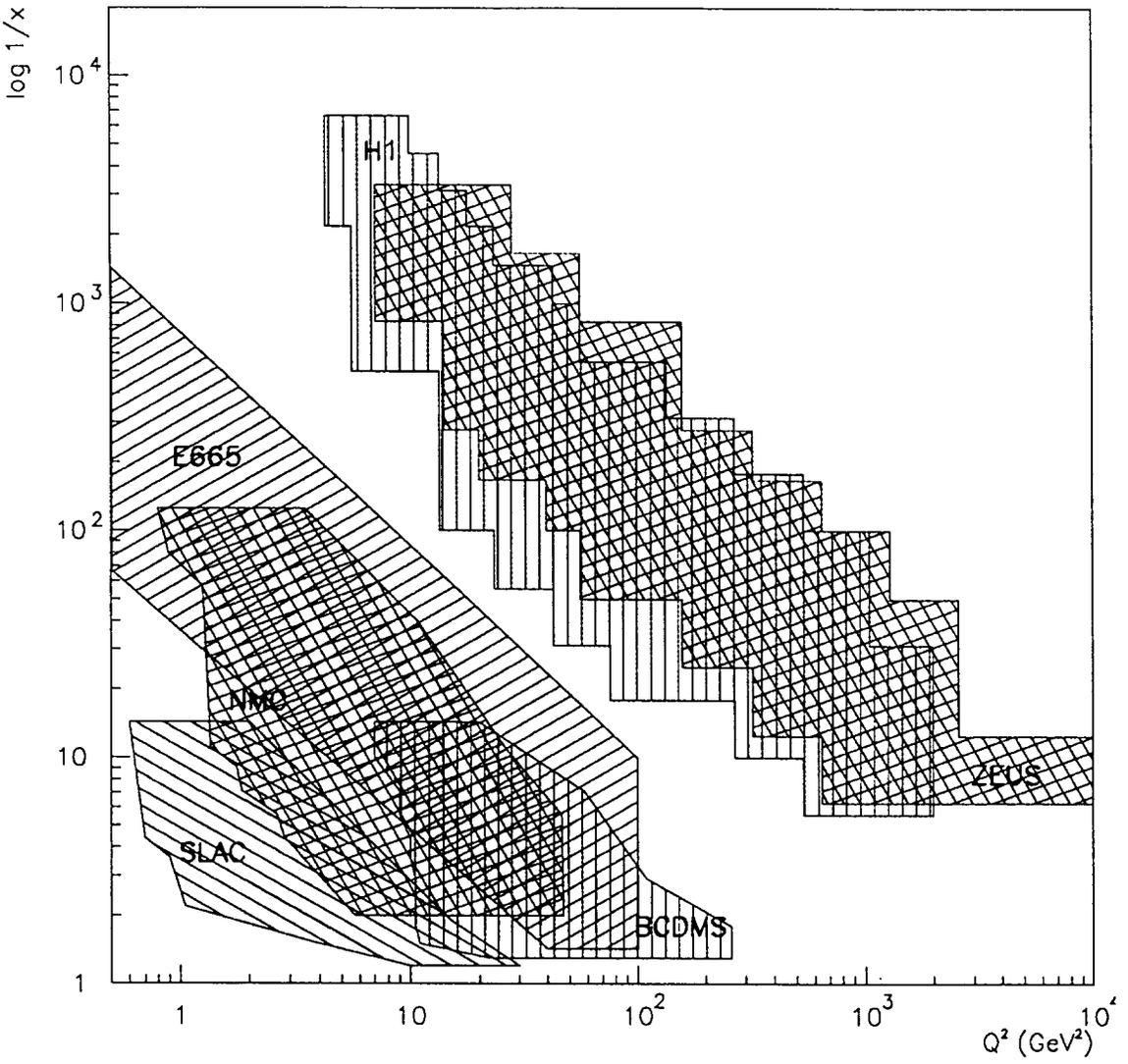

Figure 10. (x, Q^2) regions where data from fixed target (BCDMS, E665, NMC, SLAC) and HERA (H1, ZEUS) exist.

ues [24]. The validity of this parametrization at low x is questionable.

4.2. HERA experiments

The first determination of the proton structure function $F_2(x, Q^2)$ at HERA in 1992, based on a recorded luminosity of about 30 nb^{-1}, has revealed the striking feature of a proton structure function rising as x decreases below 10^{-2}, for Q^2 values in the range $8 < Q^2 < 60$ GeV^2 [45, 46]. The analysis of the 1993 data based on 10 to 20 times more integrated luminosity reported by the H1 [40] and ZEUS [41] collaborations extends the kinematic range to a lower Q^2 value of 4.5 GeV^2 and to larger Q^2 values up to 2000 GeV^2 (see figure 10).

4.2.1. x and Q^2 Reconstruction During 1993 HERA collided 26.7 GeV electrons on 820 GeV protons. Deep inelastic neutral current at HERA have the very striking topology of a well isolated electron balanced in transverse momentum by one or more hadronic jets (figure 12). The x and Q^2 variables can be reconstructed from energy and angle of the scattered electron, or from energy and average angle of the hadron flow without necessarily resolving the jets, or by a combination of scattered electron and hadron flow parameters. The ultimate method is a global fit of all observed quantities, which requires a level of understanding of the detector response and of the error correlations that the experiments have not yet achieved. The methods used to reconstruct the events in 1993 are the following :

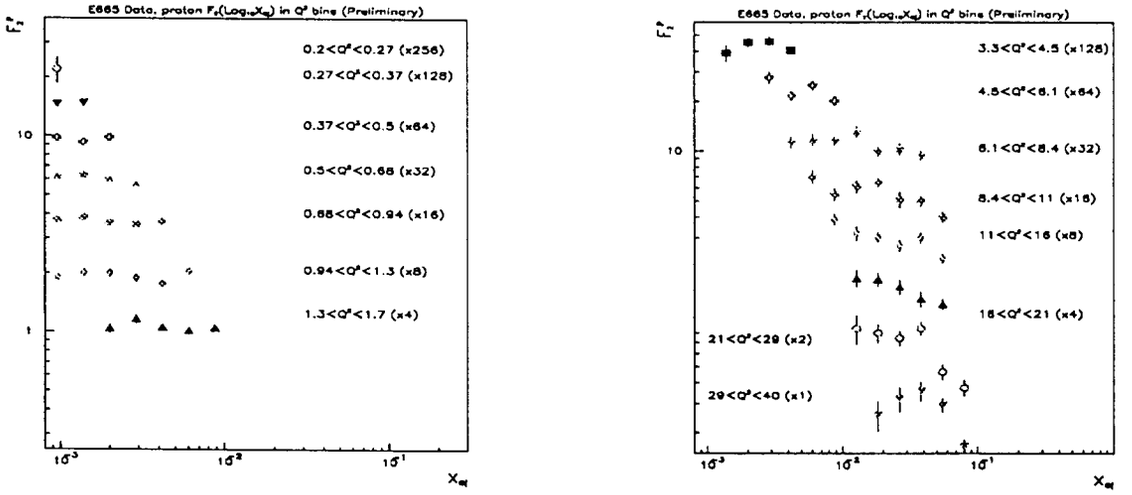

Figure 11. The structure function $F_2(x, Q^2)$ as a function of x. Preliminary results of the E665 collaboration. Only the statistical errors are shown.

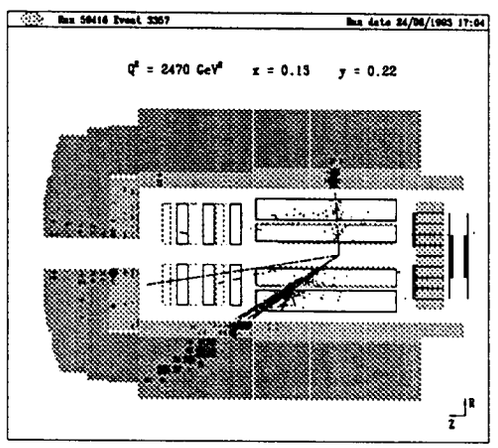

Figure 12. A neutral current deep inelastic event observed in the H1 detector. The incident electron comes from the left part. The scattered electron is easily identified as being absorbed in the first part of the calorimeter.

Electron only This is the method used so far in all fixed target experiments. It is the most precise way to reconstruct Q^2 in the whole kinematic range. But at low y ($y < 0.1$) the measurement of x is very poor [47] and at large y ($y > 0.8$) the radiative corrections to apply to the observed cross section to get the Born cross section are very large [48].

Double Angle In the Double Angle method [49] only the angles of the scattered electron and of the hadronic system are used. The method is almost independent of energy scales in the calorimeters but, at very low y, the method is very sensitive to noise in the calorimeters.

Sigma(Σ) A new method used by the H1 collaboration [40]. It combines y from the following expressions: :

$$y_\Sigma = \frac{\Sigma_h (E - P_z)_h}{(E - P_z)_e + \Sigma_h (E - P_z)_h} \tag{37}$$

where the sum runs over all hadrons in the numerator and over all hadrons plus the scattered electron in the denominator, and Q^2

$$Q^2_\Sigma = \frac{E'^2_e \sin^2 \theta_e}{1 - y_\Sigma} \tag{38}$$

where E'_e and θ_e are the scattered electron energy and angle. Here the polar angle θ_e is defined relative to the proton energy. In this method the energy of the incident electron at the interaction is reconstructed, which reduces drastically the sensitivity to the main radiative process where a real photon is emitted from the incident electron before the interaction. The resolution in x at low y is good enough to allow the H1 collaboration to reach $y = 0.01$. The resolution at large y is worse but less sensitive to the radiative corrections than when using only the parameters of the scattered electron. [40]

Experiments	Electron only	Double-Angle	Σ
H1	$y > 0.15$	cross-check	$0.01 < y < 0.15$
ZEUS	cross-check	$y > 0.03$	No

Table 4. Methods used by the H1 and ZEUS experiments to reconstruct the kinematic variables.

The methods actually used by H1 and ZEUS experiments are summarised in Table 4.

4.2.2. Systematic errors Fixed target lepton-nucleon scattering experiments have demonstrated in the past that the quality of the measurement of structure functions depend mainly on the control of the systematic effects. It has required many years before reaching errors of 5% or less. The systematic errors of the HERA experiments are currently about 10% reaching at most 25% in the worst bins. There is a long list of effects that cannot be detailed in this report. Let us briefly comment on three of the systematic effects which are specific of the HERA kinematic domain :

Radiative Corrections The dominant source of radiative corrections is emission of real photons collinear with the incident electron direction. The radiative events are largely eliminated by applying a cut on δ, the total sum on all visible particles, $\delta = \Sigma_{h+e}(E - P_z)_{h,e}$. For fully contained events $\delta \approx 2E_e = 53.4\text{GeV}$. This quantity is hardly affected by losses in the proton direction but is very sensitive to any loss in the electron direction. The radiative corrections can also be reduced when the energy of the incident electron is not used to reconstruct the kinematics as in the Double Angle and Σ methods. The corrections have been determined after simulations of the leading log radiative processes in the detectors [50]. The detailed simulations have been cross-checked by analytical calculations [51]. The predictions have even been tested directly with events where the real photon is actually measured in a photon detector, installed 100 m downstream of the interaction point along the electron beam direction. In the acceptance domains of H1 and ZEUS, $y < 0.7$ at low x, the corrections are below 10%. The radiative corrections do not contribute significantly to the overall systematic errors.

Photoproduction Background The main source of background for DIS events is photoproduction at low Q^2 and high y, where the electron scatters through a small angle, remains in most cases undetected in the beam pipe, but transfers a substantial fraction of its energy to the hadronic final state. A photon or a low energy charged pion or a superposition of both may mimic a scattered electron and thus contaminate the DIS sample. Close to the beam pipe, in a high multiplicity environment, the identification is especially difficult. As the ratio of cross-sections of DIS events at $Q^2 > 5$ GeV^2 to photoproduction events is about a factor 1000 and concentrated in the high y bins, it is a serious source of contamination of up to 15%. In each bin the background is estimated from Monte-Carlo simulations of photoproduction events. The corrections have been checked by several methods which agree to within 50% of the applied correction. H1 and ZEUS are presently upgrading their detectors to improve the rejection of this background.

$R(= \sigma_L/\sigma_T)$ The contribution from the longitudinal structure function to the cross-section (Equation (36)) has been corrected according to perturbative QCD expectations which have been calculated using F_2 parametrizations close to HERA data at low x but where the gluon density is not yet constrained by the data. The largest contribution reaches 15% at high y and low x. No errors are quoted by the experiments for this systematic effect. A high precision determination of F_2 requires a measurement of R in the HERA domain.

In addition, there are the usual many systematic contributions related to the understanding of the detector response, namely efficiency, resolution and calibration. Most of the sources of systematic uncertainties contribute differently to the structure function F_2 after reconstruction of the kinematics by the different methods given in Table 4. In the H1 and ZEUS analyses the agreement between the various determinations of F_2 has been found to be well within the quoted sytematic errors.

4.2.3. Results The results on $F_2(x, Q^2)$ from H1 and ZEUS are shown in figure 13 as a function of x at fixed Q^2 values. The overall normalisation errors of 3.5% and 5% for ZEUS and H1 respectively † are not shown in the figure. In all the bins where the comparison is possible the two data sets agree within the errors. The luminosity used by H1 and ZEUS amount to 0.27 pb^{-1} and 0.54 pb^{-1} respectively. The difference is mainly due to

† The normalisation uncertainty from H1 was 10% at the time of this conference and has now been reduced to 5%.

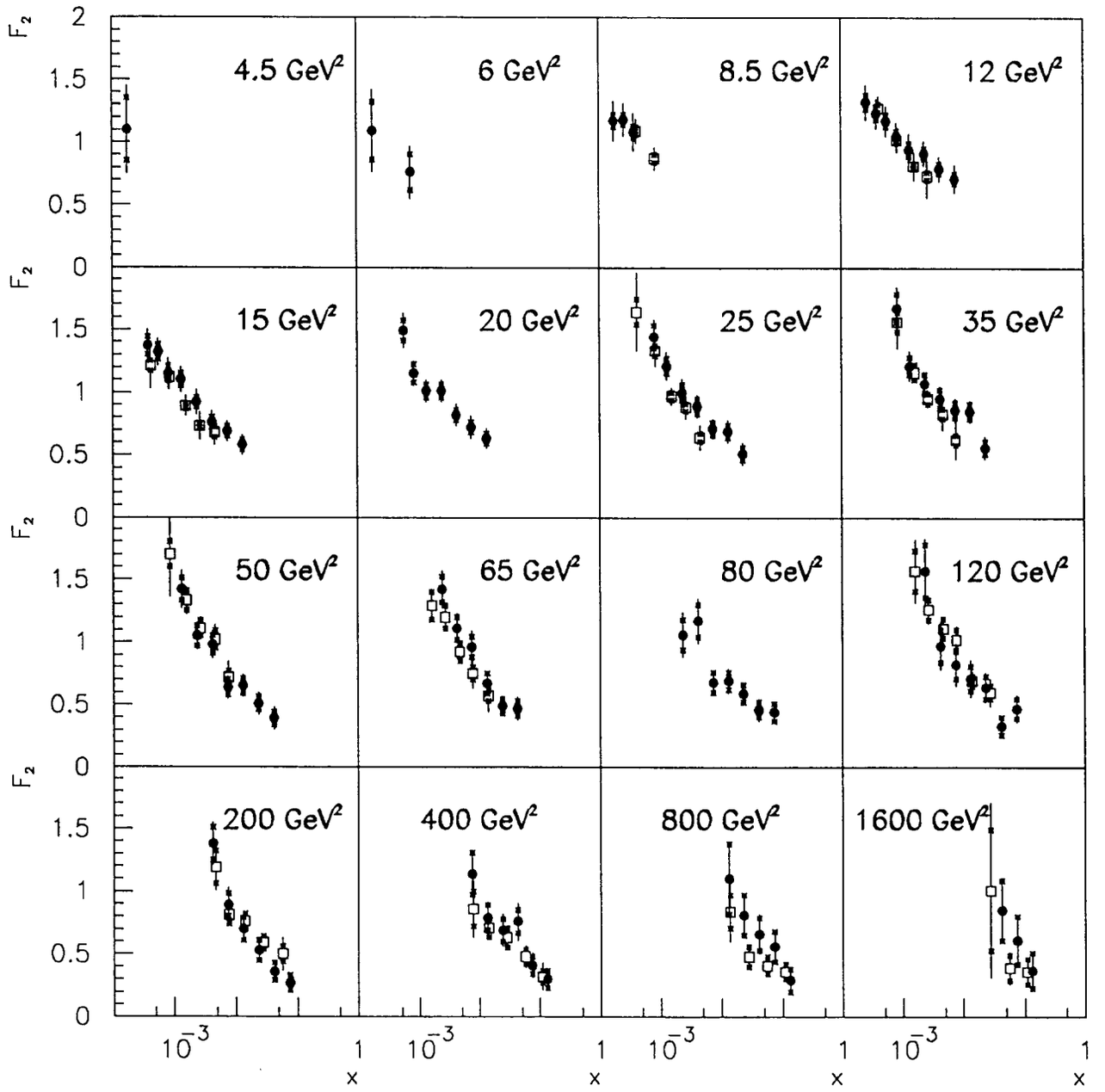

Figure 13. $F_2(x, Q^2)$ at fixed Q^2 values as a function of x from H1 (preliminary) and ZEUS experiments. The error bars show statistical and total errors obtained by adding the statistical and systematic errors in quadrature. No rebinning was made. The indicated Q^2 values are those from H1 points. The low Q^2 values from ZEUS are identical to those of H1 up to $Q^2 = 80$ GeV^2. The Q^2 values of 120, 200, 400, 800, 1600 GeV^2 of the H1 points correspond to values of 125, 250, 500, 1000, 2000 GeV^2 for the ZEUS points respectively.

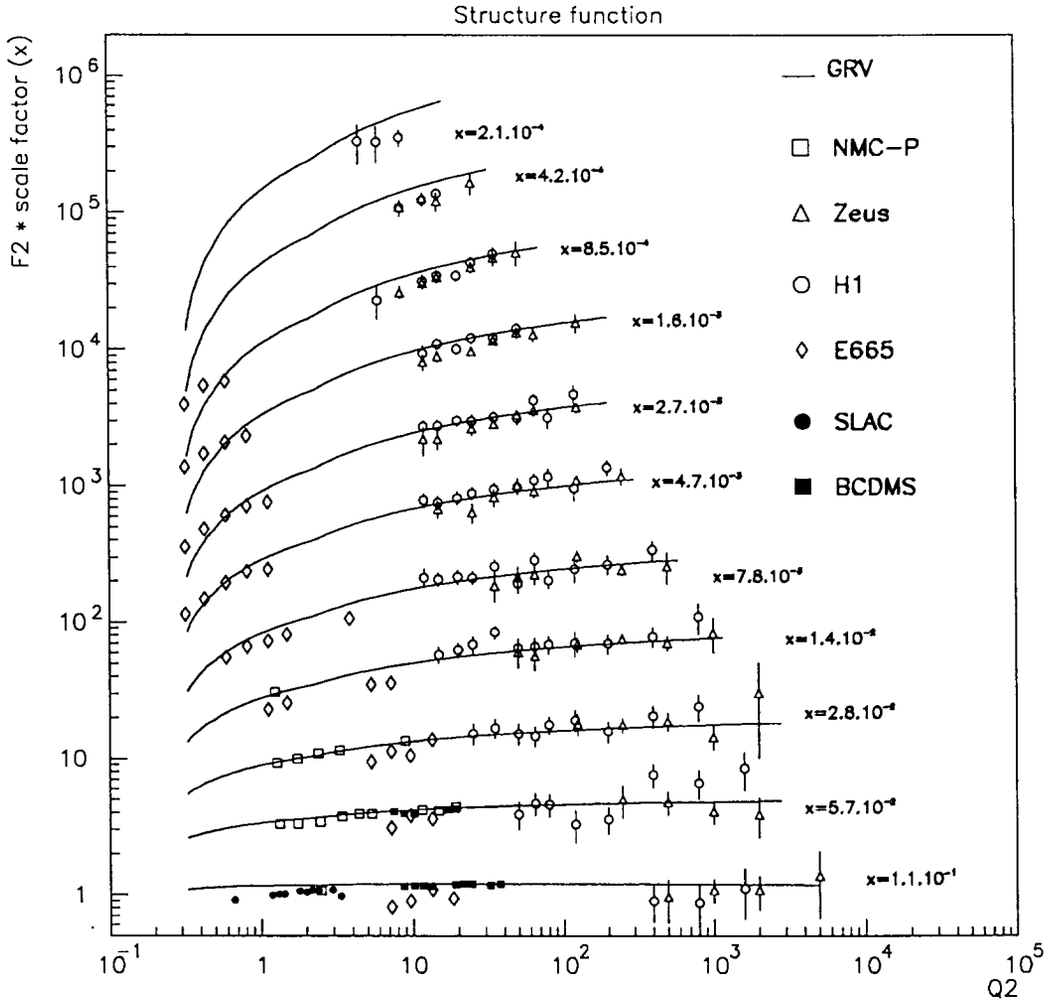

Figure 14. $F_2(x,Q^2)$ at fixed x values as a function of Q^2 from H1 (preliminary) and ZEUS together with data points from E665 (preliminary), NMC and BCDMS in the same x bins as HERA experiments. Data points of fixed target experiments have been slightly rebinned in x to match the HERA values. The error bars show the total errors, except those of E665 which are ony statistical. For clarity of the picture, common factors which are different for the different x values have been applied to all data sets.

a failure of the solenoid magnet of H1 during the most efficient period of running of HERA in September 1993. This difference reflects only in high Q^2 bins where the statistics are still the dominating source of errors. The H1 collaboration has also recorded events from a special run (2.5 nb^{-1}) where the interaction vertex was shifted by 80 cm in the proton direction to get access to smaller scattering angle of the electron. These data extend the measurable region down to Q^2 values of 4.5 GeV^2.
The steep rise of F_2 with x decreasing, observed in 1992, is well confirmed at $x < 10^{-2}$ and $Q^2 < 60$ GeV^2. In the data from 1993 the rise of F_2 is now visible up to Q^2 values of about 1000 GeV^2 and at x values below 10^{-1}.

In figure 14 the new data from HERA and E665 are shown as a function of Q^2 at fixed x and compared to fixed target experiments and to the GRV parametrization [52]. The HERA data agree with a smooth extrapolation from SLAC, BCDMS, NMC and E665 data as well as with the GRV parametrization. Positive scaling violations are clearly visible at low x and are more and more pronounced as x decreases. Furthermore one can observe in this plot that the very preliminary E665 points seem to be systematically below the previous measurements on fixed target and that at $Q^2 < 0.5$ GeV^2 the GRV parametrization is above the E665 points by up to

a factor two. It will be interesting to see whether these discrepancies persist in the final data of E665 after evaluation of the systematic errors.

4.3. Gluon determination

Based on the Gribov Lipatov Altarelli Parisi (GLAP) evolution equations [53], the behaviour of $\frac{\partial F_2}{\partial(\log Q^2)}$ can be used to extract the gluon density in the proton. At next-to-leading order (NLO) the prediction is :

$$\frac{\partial F_2(x)}{\partial(\log Q^2)} = \int_x^1 F_2(x/z)K_q(z)dz + \Sigma_q e_q^2 \int_x^1 xg(x/z)K_g(z)dz/z \quad (39)$$

where the sum runs over flavours and antiflavours and e_q is the electric charge of quark q. The splitting functions K_q and K_g are known fully to next-to-leading order in α_s. Several methods have been used to deconvolute the gluon density :

Prytz Neglecting the quark contribution and doing a Taylor expansion of the splitting function around $x = \frac{1}{2}$, Prytz [54] has obtained a very simple LO expression of the gluon density :

$$xg(x,Q^2) \approx \frac{27\pi}{20\alpha_s(Q^2)} \frac{\partial F_2(\frac{x}{2},Q^2)}{\partial \log Q^2} \quad (40)$$

It is a crude approximation which holds to within 20% at $x = 10^{-3}$ [55]. Approximate NLO corrections have been calculated [56, 57].

Ellis-Kunstz-Levin The method consists of solving the GLAP evolution equation in momentum space [58]. This leads to the following relation,

$$xg(x,Q^2) = f_1 \otimes \frac{\partial F_2(x,Q^2)}{\partial(\log Q^2)} + f_2 \otimes F_2(x,Q^2) \quad (41)$$

where f_1 and f_2 are known functions to fourth order in α_s and depend on the slope of F_2 in x. The relation is only valid when F_2 has a steep rise at low x.

Global fit Using parametrized forms of the x behaviour at $Q_0^2 = 5$ GeV^2 for F_2 and of the gluon density and assuming that the Q^2 evolution is given by GLAP equations, H1 and ZEUS have obtained good fits of their F_2 points and determined a parametrization of the gluon density.

Gluon determinations at LO (H1) and at NLO (ZEUS) are shown in figure 15 and figure 16 respectively. The errors are still large but the message is clear, at $Q^2 = 20$ GeV^2 the gluon distribution rises by about a factor 5 to 10 as x decreases from 10^{-1} to 10^{-3}. It exhibits a $x^{-\lambda}$ behaviour with $0.2 < \lambda < 0.5$. The NLO gluon data have also been compared to the $MRSD'_0$ and

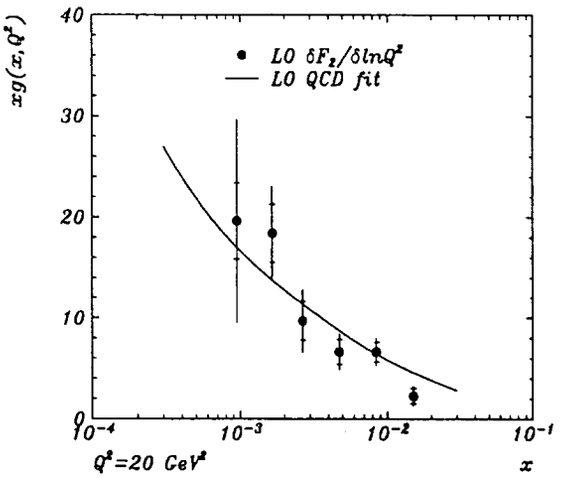

Figure 15. Preliminary gluon density $xg(x,Q^2)$ from the H1 collaboration. The full line is a leading order (LO) QCD fit. The data points are from an analysis of the scaling violation with the Prytz approximation (see text).

$MRSD'_-$ parametrizations. The two parametrizations describe the fixed target data but are based on different assumptions for the gluon input distribution at low x and $Q^2 = 5$ GeV^2. The $MRSD'_0$ assumes a flat behaviour in x while the $MRSD'_-$ assumes a singular behaviour in $x^{-0.5}$. The gluon data disfavour the $MRSD'_0$ parametrization which was already ruled out by the 1992 HERA results on F_2 [45, 46].

5. Low x Phenomenology.

The rise of the structure function F_2 at low x appeared to some as a surprising result [59] because it is in clear contrast to all previous measurements in the same Q^2 range but at larger x values †. However, a long time ago, calculations based on the operator product expansion and the renormalization group predicted that the nucleon structure function at large Q^2 and low x should grow faster than any power of $\log\frac{1}{x}$ but slower than any inverse power of x [60]. The rise was predicted to be so large that a damping mechanism should show up [61] at very low x. At present different approaches to perturbative QCD are in competition to explain the steep rise of F_2 with decreasing x.

† Although it could have been anticipated from the latest data from NMC [43].

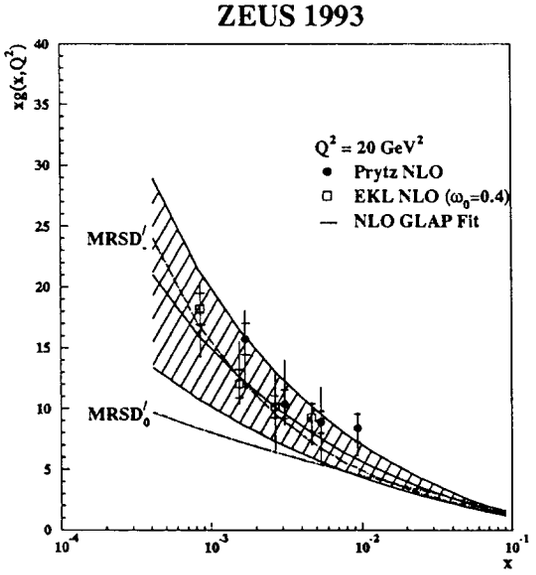

Figure 16. Preliminary gluon density $xg(x, Q^2)$ from the ZEUS collaboration as obtained by methods explained in the text. In the EKL method it is assumed that F_2 behaves in $x^{-\omega_0}$ with $\omega_0 = 0.4$. Also shown are the Martin Roberts Stirling parametrizations $MRSD'_-$ and $MRSD'_0$.

5.1. GLAP Mechanism

Given a phenomenological input function of x at some reference scale, typically $Q_0^2 = 5$ GeV^2, the well known Gribov Lipatov Altarelli Parisi (GLAP) evolution equations predict the structure function at large Q^2. The Q^2 evolution has been succesfully tested in fixed target experiments for $x > 0.01$ [63] and more recently for the HERA data at low x provided the input distributions have a steep rise at small x [64, 41]. The $MRSD'_-$, $MRSA$ and $CTEQ(2pM)$ parametrizations of parton distributions are examples of this type of behaviour [12]. Test of the GLAP evolution equations in the HERA kinematical domain has not yet reached the same level of precision as in fixed target experiments, because there has been so far no direct test of the predicted Q^2 slope but only a global fit of the x and Q^2 dependences from which χ^2 is dominated by the unpredicted x dependence.

A more ambitious approach is to start the Q^2 evolution at a very low reference scale, $Q_0^2 = 0.25$ GeV^2 [52] or $Q_0^2 = 1$ GeV^2 [62], with a non-singular input distribution, for example flat or valence-like, and to generate radiatively the parton distribution according to the GLAP evolution equations. The GRV parametrization is illustrative of this approach. It gives a good description of the data (figure 14) down to Q^2 values of about 1 GeV^2, although from a theoretical point of view it may be questionable to neglect higher twist contributions at such low Q^2 values. An interesting feature is that the structure function should exhibit asymptotic scaling in the two variables $\sqrt{(\log 1/x)(\log\log Q^2)}$ and $\sqrt{(\log 1/x)/(\log\log Q^2)}$ at sufficiently large Q^2 and low x values. Within the present errors, the H1 data provide a confirmation of both of these scaling properties (figure 17).

The GLAP evolution mechanism applied to a non singular input distribution at a reference scale $Q_0^2 \leq 1$ GeV^2 or to a singular input distribution at $Q_0^2 = 5$ GeV^2 give a good description of the HERA data. However it is based on a summation of all leading $(\alpha_s \log Q^2)^n$ contributions, but omits the summation of large $\log 1/x$ contributions which are not accompanied by large $\log Q^2$ terms, an approximation which is not supposed to hold at very low x.

5.2. BFKL Mechanism

A different mechanism is to resum the $(\alpha_s \log 1/x)^n$ terms. To leading order in $\log 1/x$ the summation is accomplished by the Balitski Fadin Kuraev Lipatov (BFKL) equation. When the effect of the running coupling constant is neglected, i.e. in a small range of Q^2, the BFKL evolution equation of the gluon can be solved analytically. The solution exhibits a Regge type $x^{-\lambda}$ dependence with

$$\lambda = \frac{12\alpha_s}{\pi} \log 2 \approx 0.5 \qquad (42)$$

The quantity $1 + \lambda$ is equal to the intercept of the so called BFKL hard pomeron which is very different from the 1.08 intercept of the effective soft pomeron which describes so well the energy dependence of all hadron-hadron and photon-hadron cross sections [66]. When the running of α_s is taken into account the exponent λ is expected to be a bit smaller [67, 68, 70] . The present crude determination of the gluon density supports the BFKL prediction of a $x^{-\lambda}$ steep rise at low x.

For completeness we should also mention that the rise of the gluon density has to be damped at some sufficiently small value of x by saturation (shadowing) effects when the parton density is so large that the partons can no longer be considered as independent. The Gribov Levin Ryskin (GLR) equation is the first attempt to describe the shadowing correction to the BFKL linear evolution equations. It is a perturbative QCD calculation applied in the transition region to the unknown domain of non-perturbative QCD. Shadowing effects are however expected to be relatively weak in the HERA kinematical domain [69, 70, 71].

The theory cannot predict so far the precise domains of validity of the different approaches. There is no scale in the $\log Q^2$-$\log \frac{1}{x}$ map of the evolution mechanisms

(figure 18). This is the task of the experiments but the present measurements of F_2 are compatible with both the BFKL and GLAP mechanisms and cannot reveal the underlying dynamics. The properties of the hadronic final state which accompany the deep inelastic scattered electron are however anticipated to be a better discriminator between the two mechanisms [72].

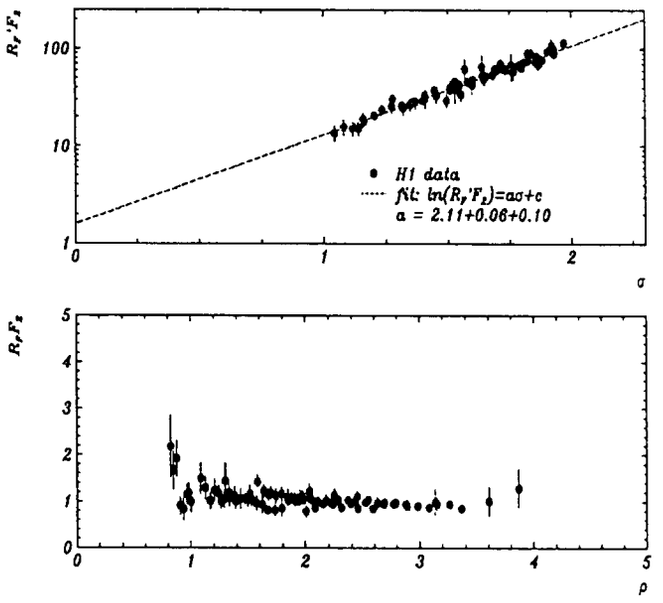

Figure 17. The rescaled structure functions $R'_F F_2^p$ and $R_F F_2^p$ plotted against σ and ρ where $\sigma = \sqrt{\log \frac{x_0}{x} \log \frac{t}{t_0}}$, $\rho = \sqrt{\log \frac{x_0}{x} / \log \frac{t}{t_0}}$ and $t_0 = \log Q_0^2/\Lambda^2$. The starting values are $x_0 = 0.1$ and $Q_0^2 = 1$ GeV^2. R_F and R'_F are simple rescaling factors to remove the trivial model-independent part of the prediction. The data points from H1 are preliminary. The fitted slope a is to be compared with the predicted slope of 2.4 [62].

5.3. *Hadronic Final State*

In an axial gauge the resummation of leading $(\alpha_s \log Q^2)^n$ contributions, as in the GLAP evolution, comes from the diagram with n rungs of gluons (figure 19) with ordered longitudinal momenta and strongly ordered transverse momenta along the ladder, that is :

$$\begin{aligned} Q^2 \gg k_{nt}^2 \gg \ldots \gg k_{1t}^2 \\ x > x_1 > \ldots > x_n \end{aligned} \qquad (43)$$

This is in contrast to the BFKL evolution where there is no restriction on transverse momenta in the summation but a strong ordering in longitudinal momenta :

$$\begin{aligned} Q^2 > k_{nt}^2 > \ldots > k_{1t}^2 \\ x \gg x_1 \gg \ldots \gg x_n \end{aligned} \qquad (44)$$

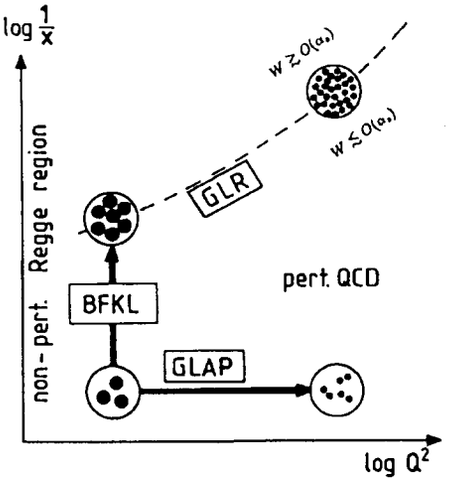

Figure 18. Schematic evolution of the quark densities in various (x, Q^2) regions according to the dominant dynamical effects. The dashed line is the theoretical limit of validity of perturbative QCD. (Picture nicely provided by A.D. Martin.)

The H1 collaboration has studied two processes which exploit this behaviour.

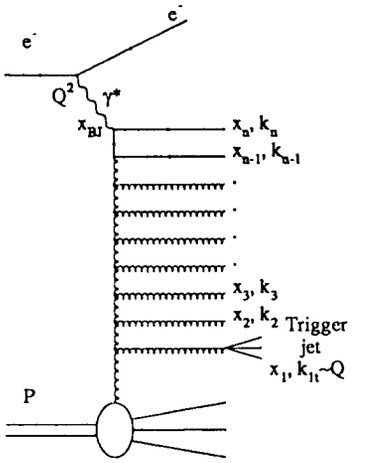

Figure 19. Diagrammatic representation of the gluon rungs contributing to deep inelastic scattering. The selection of a forward jet may be a way of identifying BFKL dynamics.

5.3.1. Transverse Energy Flow In the naive quark-parton model the transverse momentum of the scattered electron is balanced by a single jet associated with the struck quark called the current jet. Higher-order QCD processes generated by GLAP or BFKL mechanisms modify this picture. Expectations for the properties of hadronic final states are available in the form of Monte Carlo models or analytic calculations. The Monte Carlo models are based on GLAP QCD evolution but differ widely in their predictions. The MEPS model is an option of the LEPTO generator [73] based on GLAP dynamics [53]. It combines rigorous LO matrix elements and an approximate treatment of higher order effects with leading-log parton showers. The CDM model [74] provides an implementation of the colour dipole model of a chain of independent radiating dipoles connected via the emitting gluons. It is however argued that the colour dipole description emulates BFKL behaviour to some extent [68, 75].

The transverse energy flow in the laboratory system, corrected for detector effects, is shown in figure 20 as a function of the pseudorapidity †. in the laboratory system. It is a study based on data recorded in 1992 which corresponds to an integrated luminosity of 22.5 nb^{-1} [76] At $x < 10^{-3}$ the H1 data show a peak from the current jet and a plateau of $E_T \approx 2$ GeV per unit of rapidity between the current jet direction and the proton remnant. The MEPS model gives too little transverse energy away from the current jet. The CDM model is in reasonable agreement with the data. The high value of E_T has also been compared with analytic calculations [77] based on BFKL dynamics which predict a fairly flat plateau at low x with $E_T \approx 2$ GeV per unit of rapidity but much less E_T if GLAP dynamics is assumed (figure 21). However this is not yet conclusive evidence because no hadronization has been included in the analytic calculations.

5.3.2. Forward jets in DIS events Further possible evidence for BFKL dynamics is the rate of jets produced in the proton direction as sketched in figure 19. In order to be more sensitive to BFKL dynamics, the transverse size $1/k_{jt}$ of the selected jet should be close to $1/Q$ and the momentum fraction x_j of the jet should be as large as possible and the momentum fraction x of the quark struck by the virtual photon should be as small as possible. Jets with square transverse momenta $k_t^2 \approx Q^2$ leave little phase space in the cascade for GLAP evolution, and requiring $x_j \gg x$ opens a large space for BFKL evolution. Thus the expected rates should be enhanced according to the BFKL mechanism [78].

In a sample of DIS events with $Q^2 \approx 20$ GeV^2 and

† Pseudorapidity $\eta = -\log(\tan\frac{\theta}{2})$ with the polar angle θ measured relative to the proton direction

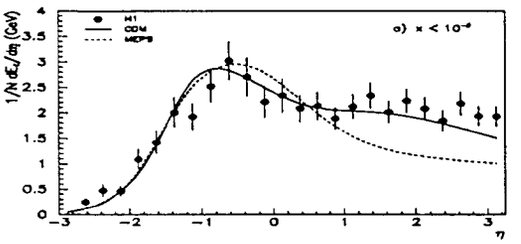

Figure 20. Transverse energy as a function of pseudorapidity η in the laboratory system. The proton direction is to the right. Fully simulated MEPS and CDM expectations are compared with H1 data at $< x >= 5.7\ 10^{-4}$ and $< Q^2 >= 15\ GeV^2$.

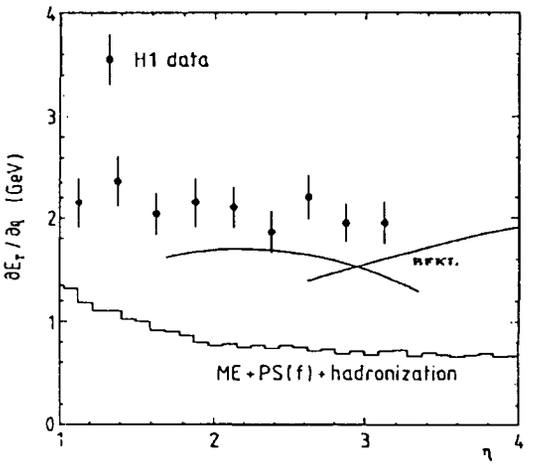

Figure 21. Transverse energy as a function of the pseudorapidity η in the laboratory system. The proton direction is to the right. Analytic calculations are compared to the H1 data of the previous figure.

$2 \cdot 10^{-4} < x < 2 \cdot 10^{-3}$, H1 has counted jets with $x_j > 0.05$ and $0.5 < k_{jt}^2/Q^2 < 6$. The resulting number of events, corrected for background contribution, is given in Table 5 and compared with the expectations of the MEPS and CDM models fully simulated in the H1 detector. We can see that the predictions tend to be below the observations and do not depend significantly on the parametrization of structure functions ($MRSD0$ [4] or $MRSD^-$ [5]). The size of the errors do not allow yet any firm conclusion. We can however notice that the rate of jets rises with decreasing x as expected in BFKL dynamics [78].

5.3.3. Other possible processes Other processes have been proposed to identify BFKL dynamics :

x range	Data	MEPS $MRSD0$	MEPS $MRSD^-$	CDM
0.0002 – 0.001	$85 \pm 9 \pm 17$	37	27	32
0.001 – 0.002	$43 \pm 7 \pm 9$	32	26	21

Table 5. Number of DIS events with a selected forward jet.

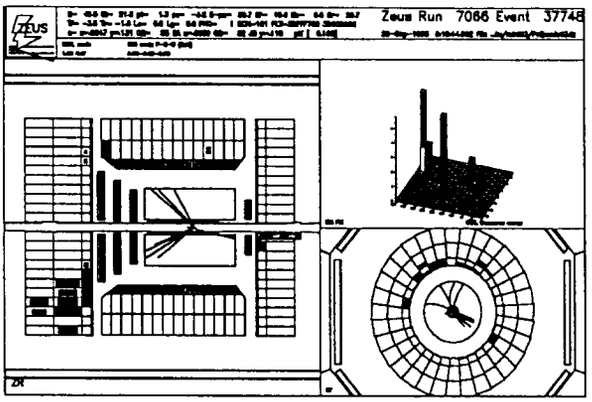

Figure 22. Display of a deep inelastic event with a large rapidity gap observed in the ZEUS detector. There is no energy deposited in a large region of rapidity in the proton direction, that is to the left in the figure.

- weakening of the azimuthal correlation between a pair of jets produced in deep inelastic scattering at low x [79].
- rapidity dependence of the cross section for the production of a pair of minijets. It is anticipated that the rate should rise as the rapidity interval between the minijets becomes large [80, 81, 82].

These ideas have not yet been confronted with the HERA data. In summary, there is not yet a firm conclusion but it seems that measurements less inclusive than F_2 offer a good chance to identify the BFKL mechanism.

6. Diffraction in deep inelastic scattering.

It was anticipated that the HERA collider should provide a rather unique possibility to study diffractive dissociation at short distances [83] and that the rapidity gap would be a powerful criterion to eliminate conventional deep inelastic background. Analysing the 1992 data, the ZEUS and H1 collaborations [84, 85] have found deep inelastic events in which no energy flow is observed in a large region of rapidity close to the proton direction, as illustrated in figure 22. The events

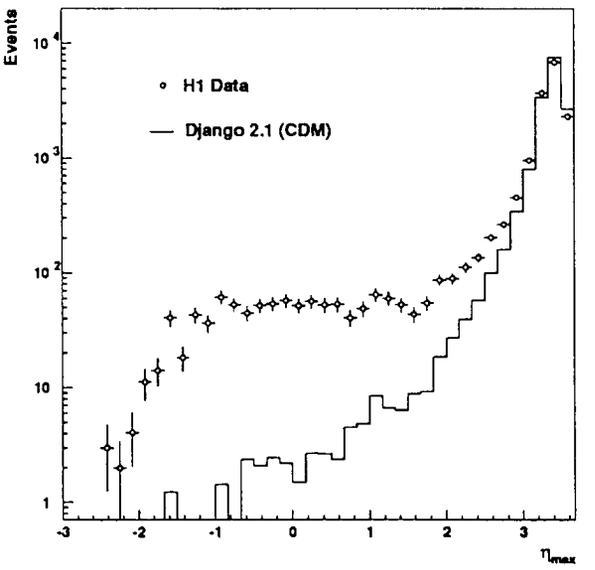

Figure 23. Distribution of measured η_{max} for all DIS events together with the expectation from the standard DIS model based on the DJANGO simulation (LEPTO + radiative processes).

exhibit a sizeable difference, the so called rapidity gap, between the pseudorapidity of the most forward part of the detector and η_{max} the largest rapidity of particles observed in the event. The rate of events with a small η_{max} is largely above the expectations of standard DIS models [86] (figure 23).

Assuming that the proton interacts diffractively, the interaction can be modelled as the exchange of a colourless Regge pole, the pomeron. Several possible mechanisms are considered, as follows :

The first mechanism, based on vector meson dominance of the photon (VMD), is leptoproduction of vector mesons, which can be elastic (figure 24 a) or followed by soft dissociation of the vector meson (figure 24 b) or by soft dissociation of the proton (figure 24 c).

The second mechanism considers the possibility that any partonic structure of the pomeron, a quark (figure 24 e) or a gluon (figure 24 f), is resolved by the high Q^2 photon [87]. A hard partonic structure of the pomeron can explain the high p_T jets observed in diffractive $\bar{p}p$ interactions [88]. The model has been implemented in simulation programs where the parton momentum density in the pomeron is an arbitrary input to be confronted with the data [89, 90].

The third mechanism assumes that the exchanged virtual photon fluctuates into a quark-antiquark pair which interacts with a colourless two-gluon system emitted by the incident proton [91].

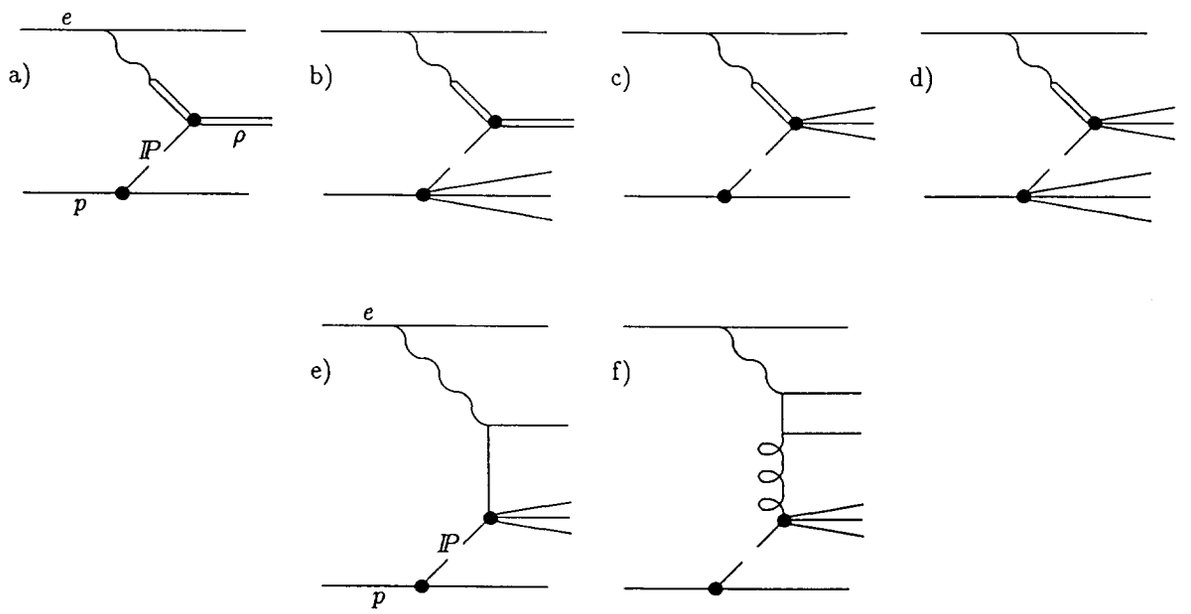

Figure 24. Diagrams which illustrate the VMD and deep inelastic electron pomeron scattering descriptions of the rapidity gap events: a) ρ production via elastic VMD; b) VMD ρ production with soft dissociation of the proton; c) VMD photon interaction followed by soft dissociation of the vector meson; d) VMD photon interaction followed by soft dissociation of both the vector meson and the proton; e) inelastic scattering off a quark in the pomeron; f) inelastic scattering off a gluon in the pomeron via photon gluon fusion.

The shape of the low η_{max} ($\eta_{max} < 1.5$) distribution can be equally reproduced by a VMD motivated simulation [92] or by a a simulation of electron-pomeron scattering [92, 94].

The observed fraction of rapidity gap events in the DIS sample amounts to about 5%. However the cut on η_{max} has selected only part of the diffractive events. After acceptance correction which depends on the models used to describe the events, the H1 and ZEUS experiments get an estimate of the corrected fraction of diffractive events in the DIS sample which varies between 10 and 15 % [92, 95]. The rapidity gap events at HERA are distributed over the entire Q^2 and x range covered by the whole sample of DIS events. Figure 25 shows the ratio of rapidity gap events to all DIS events as a function of Q^2 in narrow x regions as measured by the ZEUS collaboration. The data are restricted to values of $W > 140$ GeV where Monte Carlo calculations have shown that the acceptance is flat in Q^2. It is striking that this ratio has no significant dependence on Q^2, which is consistent with a leading twist QCD production mechanism. The similarity in the Q^2 dependence of rapidity gap events with normal DIS events is as expected in models based on partonic structure of the pomeron. However given the uncertainties in the Q^2 dependence of VMD models for highly virtual photons it is possible to reproduce the ratio observed in figure 25 in a VMD-like picture [92].

The rapidity gap events contribute to the inclusive measurement of the structure function F_2. Following [93] it is possible to define a diffractive structure function f_2^D :

$$\frac{d\sigma(ep \to epX)}{dx_{I\!P}dtdxdQ^2} = \frac{2\pi\alpha^2}{Q^4 x}\left(2\,(1-y) + y^2\right) f_2^D(x, Q^2, x_{I\!P}, t) \qquad (45)$$

where the contribution of the longitudinal structure function has been neglected. Here $x_{I\!P}$ is the fraction of the proton energy carried by the pomeron and t is the square momentum transfer between the incident and the outgoing proton. The integral of f_2^D over $x_{I\!P}$ and t gives the contribution from the diffractive events to the structure function $F_2(x, Q^2)$ that we call F_2^D :

$$F_2^D(x, Q^2) = \int f_2^D(x, Q^2, x_{I\!P}, t) dx_{I\!P} dt \qquad (46)$$

There is however a strong correlation between the rapidity η_{max} and the variable $x_{I\!P}$ (figure 26). In the H1 analysis a cut on $\eta_{max} < 1.8$ selects mainly events with $x_{I\!P} < 0.01$ and hence with $x < 0.01$ because the variables x and $x_{I\!P}$ are trivially related by :

$$x = x_{I\!P}\frac{Q^2}{Q^2 + M_X^2} \qquad (47)$$

where M_X is the invariant mass of the final state hadronic system excluding the scattered proton. The

resulting diffractive structure function $F_2^D(x,Q^2)$ for $x_{I\!P} < 0.01$ is shown in figure 27 together with the total inclusive structure function $F_2(x,Q^2)$. For $x < 10^{-3}$, $F_2^D(x,Q^2)$ contributes to about 10% to $F_2(x,Q^2)$. Clearly the diffractive events cannot explain the rise of F_2 at low x. The x dependence of F_2^D at x approaching 10^{-2} has to be considered with caution, because the cut on $x_{I\!P} < 0.01$ forces F_2^D to zero at $x = 10^{-2}$.

An important characteristic of models in which the pomeron has a partonic structure, is the factorization of f_2^D into a pomeron flux term and a pomeron structure function :

$$f_2^D(x,Q^2,x_{I\!P},t) = f(x_{I\!P},t)F_2^{I\!P}(z,Q^2) \qquad (48)$$

where $z = \frac{x}{x_{I\!P}}$ and $f(x_{I\!P},t)$ is the pomeron flux factor. The momentum transfer t cannot be measured so far in the HERA experiments. If the factorization is true, the integral $\int f_2^D dt$ should have the same $x_{I\!P}$ behaviour independent of z and Q^2.

In a dedicated analysis, the H1 collaboration has replaced the η_{max} selection by a cut on a set of forward tagging detectors which are mainly sensitive to secondaries produced by forward going hadrons interacting in collimators close to the proton beam axis. This simple selection gives access to higher values of $x_{I\!P}$. The diffractive sample has been divided into four bins of Q^2 ($Q^2 = 8.5, 15, 30, 60$) times four bins of z ($z = 0.05, 0.2, 0.45, 0.8$). The $Q^2 = 15$ GeV^2 bins are shown as an illustration in figure 28. In all the bins the dependence of $f_2^D(x,Q^2,x_{I\!P},t)$ on $x_{I\!P}$ can be fitted by a simple expression :

$$\int f_2^D(x,Q^2,x_{I\!P},t)dt = x_{I\!P}^{\alpha} F_2^{I\!P}(z,Q^2) \qquad (49)$$

where

$$\alpha = -1.3 \pm 0.1. \qquad (50)$$

Within the present errors the diffractive cross section is compatible with factorization.

More insight into diffractive deep inelastic events can be gained by investigating the visible hadronic final state which accompanies the scattered electron. Production of vector mesons at high Q^2 has already been observed in fixed target experiments. New results fom the NMC collaboration on the production of exclusive ρ^0 and ϕ vector mesons at large Q^2 have even been reported at this conference [96]. In the HERA deep inelastic events there is also a substantial fraction of events where the visible hadronic final states only consists of two opposite charged tracks. A clear signal at the ρ mass has been observed [95, 92]. At $Q^2 = 8.6$ GeV^2, the ZEUS collaboration gets a $\gamma^* p \rightarrow \rho p$ cross section which is about 3 times larger than those of EMC [97] and NMC [98] at the same Q^2 value (figure 29). The difference is attributed to the 10 times larger total

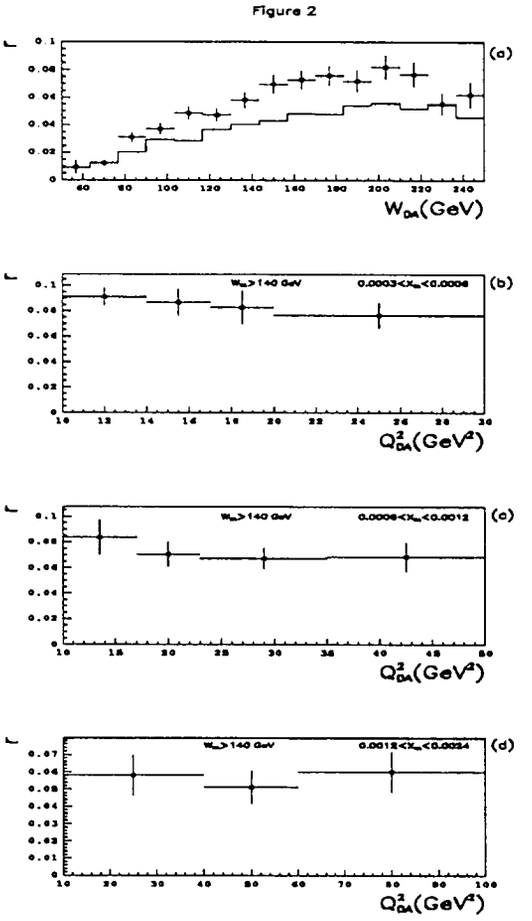

Figure 25. (a) The ratio r of the number of events with $\eta_{max} < 1.5$ to the total number of DIS events as a function of W_{DA}, the total hadronic mass measured by the double angle method (see text). The data are from the ZEUS experiment. The histogram shows the acceptance in arbitrary units. (b)(c)and (d) The ratio r for $W_{DA} > 140$ GeV for three intervals of x.

invariant hadronic mass W in the HERA kinematic range. The H1 and ZEUS analyses conclude that about 10% of the observed rapidity gap events are exclusive vector mesons. It involves however an unknown part of events where the vector meson production is associated with proton dissociation which is not observed. This part has been estimated to be 15% in Monte Carlo studies by the ZEUS collaboration.

A ZEUS analysis of the hadronic system shows also that in the laboratory frame 15% of the rapidity gap events are of the 1-jet type with $E_T^{jet} \geq 4\ GeV$ [95, 99] with a negligible 2-jet production. With a lower jet transverse energy cut of 2 GeV, a small 2-jet production is observed in the $\gamma^* p$ centre of mass frame. This is consistent with the assumption that rapidity gap events are produced in the interaction of the virtual photon

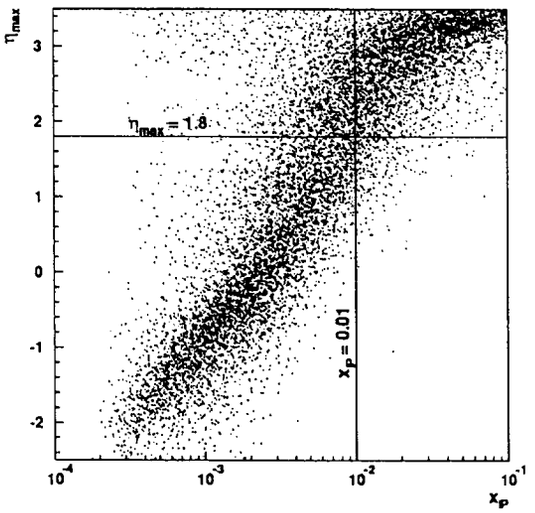

Figure 26. Correlation between η_{max} and $x_{\mathbb{P}}$ from Monte Carlo studies by the H1 collaboration.

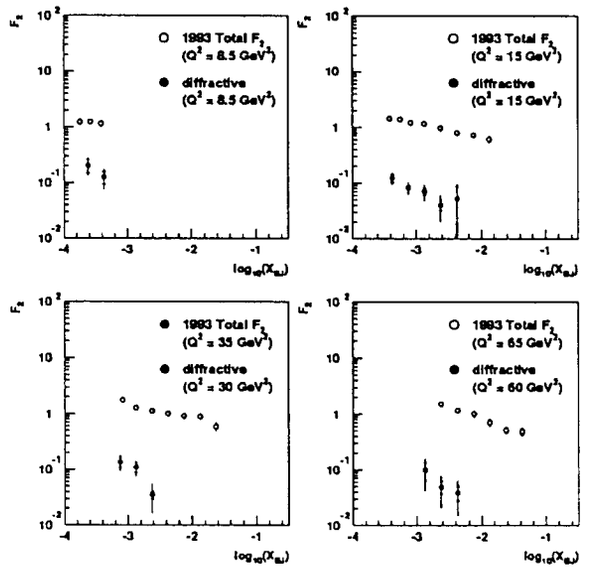

Figure 27. Contribution of the diffractive structure function $F_2^D(x, Q^2)$ for events with $x_{\mathbb{P}} < 0.01$ to the inclusive proton structure function F_2. The data points are preliminary results from the H1 experiment.

with partons in the pomeron.

The properties of the rapidity gap events in deep inelastic scattering at HERA can be summarized as follows.

- After acceptance correction, the diffractive events represent about 10% of the DIS sample.
- The Q^2 dependence is similar to all DIS events.
- The rapidity gap events cannot explain the rise of F_2.

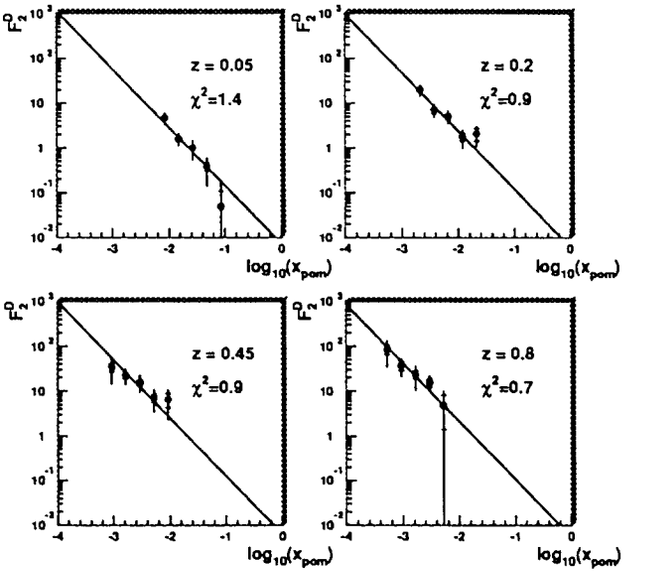

Figure 28. The diffractive structure function $f_2^D(x, Q^2, x_{\mathbb{P}}, t)$ as a function of $x_{\mathbb{P}}$ after integration over the variable t. The data points are preliminary results from the H1 experiment. The straight line is a fit of the $x_{\mathbb{P}}^{\alpha}$ behaviour with $\alpha = -1.3 \pm 0.1$.

- About 10% of the observed rapidity gap events are exclusive vector mesons with or without proton dissociation.
- In the laboratory frame 15% of the rapidity gap events are of the 1-jet type with $E_T^{jet} \geq 4\ GeV$
- The diffractive cross section can be factorized in a pomeron flux term and a pomeron structure function.

The interpretation of the events is still very open. No firm conclusion can be drawn yet.

We should also mention that in $p\bar{p}$ interactions at $\sqrt{s} = 1.8$ GeV, the CDF and D0 collaborations have identified a sample of events with a rapidity gap topology. In CDF (figure 30) an excess of trackless events in rapidity intervals between jet cones has been reported [100]. In D0 (figure 31) a very significant excess of low calorimeter tower multiplicity between the two highest transverse energy jets has been found [101]. The two observations are consistent with the exchange of a strongly interacting colour singlet as suggested by Bjorken [102].

7. Conclusion

In summary, a wealth of new results on the structure of the proton and on low x physics has been presented at this conference by fixed target and HERA experiments.

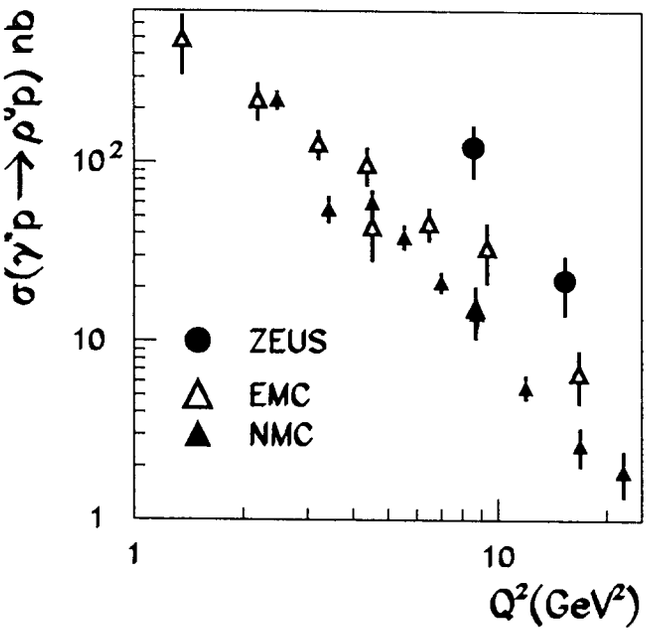

Figure 29. ρ^0 cross section for virtual photoproduction as a function of Q^2. The mean $\gamma^* p$ centre of mass energy W is about 10 GeV in the EMC/NMC data points and 100 GeVin the ZEUS data points.

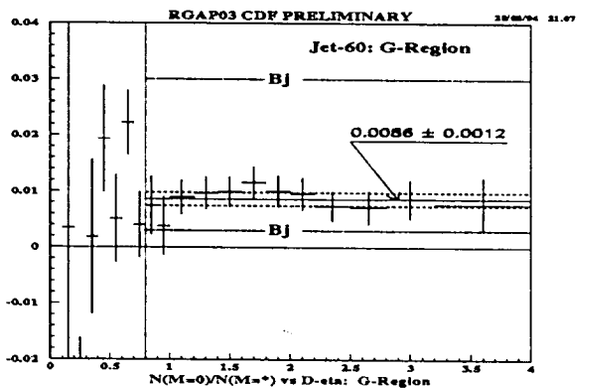

Figure 30. Ratio of the trackless events to total events as a function of the rapidity intervals between jets. The data points are preliminary results from the CDF collaboration. The average is indicated by the solid horizontal line and dashed error corridor. The prediction from Bjorken's model of colorless digluon exchange lies between 0.003 and 0.03 as indicated by the horizontal lines marked 'Bj'.

- The flavour asymmetry of the light sea quarks, $\bar{u}$ $\bar{d}$ and $\bar{s}$, is well confirmed.

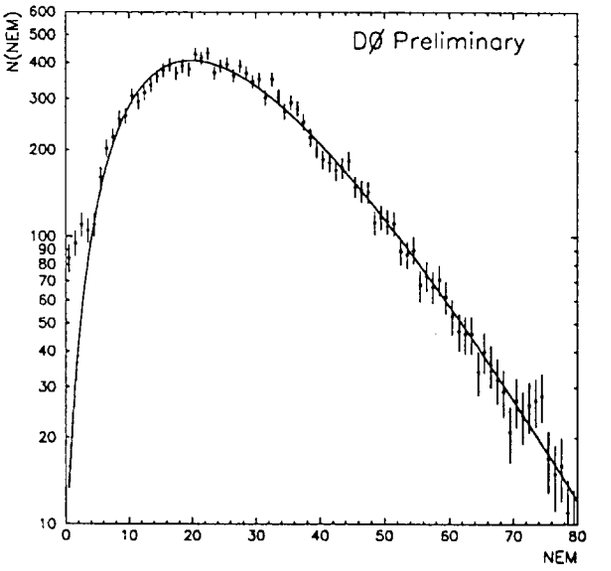

Figure 31. Distribution of multiplicity of electromagnetic towers (NEM) between the two highest transverse energy jets separated by at least three units of rapidity. The data points are preliminary results from the D0 collaboration. The solid line is a negative binomial distribution (NBD). A clear excess is visible at low multiplicities.

- There is a fair consistency between all results on polarized structure functions. The naive Ellis-Jaffe sum rule is not satisfied by the data provided the low x extrapolation to zero is not singular. The measured QCD corrections at low Q^2 to the Bjorken Sum Rule provide a new method to determine the QCD running coupling constant α_s.
- Combining fixed target and HERA results, the measurement of the proton structure function $F_2(x, Q^2)$ covers the very large kinematic range of $0.3 < Q^2 < 10^4$ GeV^2 and $2\ 10^{-4} < x < 1$. The steep rise of the structure function F_2 with x decreasing is observed at x values below 10^{-1} and up to Q^2 values of about 1000 GeV^2.
- The observed behaviour of F_2 at low x is compatible with both the BFKL and GLAP mechanisms and cannot reveal the underlying dynamics. The properties of the hadronic final state seem to favour BFKL dynamics but are not yet conclusive.
- The class of diffractive deep inelastic events deserves a special attention. These deep inelastic events cannot be described in terms of electron interactions with the partonic structure of the proton.

The field of deep inelastic lepton-nucleon scattering is of growing importance and brings more and more insight into the understanding of QCD, the theory of strong interactions.

Aknowledgements

It is a pleasure to thank all my colleagues from CDF, CERN NA41, NMC, SMC, SLAC E143, FNAL E665, ZEUS, FNAL D0 for providing me with their data and for many useful discussions. I thank specially G. Cozzika, J. Dainton, A. De Roeck, E. Elsen, C. Royon, my colleagues from H1 and E. Hughes and P. Bussey for help in preparing the manuscript. I wish to thank also M. Karliner, G. Levin and A.D. Martin for helpful conversations to clarify many theoretical points.

References

[1] E.L. Berger *et al.*, Phys. Rev. **D40** (1989) 83.
[2] CDF Collaboration, H. Budd, these proceedings.
[3] CTEQ Collaboration: J. Botts *et al.*, Phys. Lett. **B304** (1993) 159, now superseded by CTEQ2 : J. Botts *et al.* (unpublished)
[4] A.D. Martin, W.J. Stirling, R.G. Roberts, Phys. Lett. **B306** (1993) 145, Erratum Phys. Lett. **B309** (1993) 492.
[5] A.D. Martin, W.J. Stirling, R.G. Roberts, Phys. Rev. **D47** (1993) 867.
[6] A.D. Martin, W.J. Stirling, R.G. Roberts, Proc. Workshop on Quantum Field Theoretical aspects of HE Physics, Kyffhässer, Germany, eds B.Geyer and E.M. Ilgenfritz, Leipzig (1993) p.11.
[7] NMC Collaboration : E. Kabuss, these proceedings.
[8] NMC Collaboration : M. Arneodo *et al.*, Phys. Rev. Lett. **66** (1991) 2712.
[9] A.D. Martin, W.J. Stirling, R.G. Roberts, Phys. Lett. **B252** (1990) 653.
[10] S.D. Ellis and W.J. Stirling, Phys. Lett. **B256** (1991) 258.
[11] NA51 Collaboration, A. Baldit *et al.*, Phys. Lett. **B332** (1994) 244.
[12] A.D. Martin, these proceedings. and A.D. Martin, W.J. Stirling, R.G. Roberts to be published in Physical Review D50.
[13] CCFR Collaboration: A.O. Bazarko *et al.*, Columbia University Preprint Nevis R1502, submitted to Phys. Lett. B.
[14] J. Bjorken, Phys. Rev. **148** (1966) 1467 and J. Bkorken, Phys. Rev. **D1** (1970) 1376.
[15] J. Kodaira *et al.*, Nucl. Phys. **B159** (1979) 99
[16] S.A. Larin, F.V. Tkachev and J.A.M. Vermaseren, Phys. Rev. Lett. **66** (1991) 862 and S.A. Larin and J.A.M. Vermaseren, Phys. Lett. **B259** (1991) 345.
[17] A.L. Kataev and V. Starshenko, CERN-TH-7198-94.
[18] J. Ellis and R.L. Jaffe, Phys. Rev. D9 (1974) 1444; and Phys. Rev. **D10** (1974) 1669.
[19] S.A. Larin, CERN-TH-7208-94.
[20] A.L. Kataev, CERN-TH-7333-94 and these proceedings.
[21] SLAC E-80 Collaboration, M.J. Alguard *et al.*, Phys. Rev. Lett. **37** (1976) 1261 and *ibid.* **41** (1978) 70.
[22] SLAC E-130 Collaboration, G. Baum *et al.*, Phys. Rev. Lett. **51** (1983) 1135.
[23] SMC Collaboration, A. Staude, these proceedings and D.Adams *et al.*, Phys. Lett. **B328** (1994) 399.
[24] L.W. Whitlow *et al.*, Phys. Lett. **B250** (1990) 193.
[25] EMC Collaboration, J. Ashman *et al.*, Nucl. Phys. **B328** (1989) 1.
[26] J.McCarthy, these proceedings.
[27] SMC Collaboration, B. Adeva *et al.*, Phys. Lett. **B302** (1993) 533.
[28] SLAC E-142, D.L. Anthony *et al.*, Phys. Rev. Lett. **71** (1993) 959.
[29] J. Ellis and M. Karliner, Phys. Lett. **B313** (1993) 131.
[30] F.E. Close and R.G. Roberts, Phys. Lett. **B316** (1993) 165.
[31] G. Altarelli *et al.*, Phys. Lett. **B320** (1994) 152.
[32] SMC Collaboration, B. Adeva *et al.*, Phys. Lett. **B320** (1994) 400.
[33] J. Ellis and M. Karliner, CERN-TH-7324/94.
[34] B. Webber, these proceedings.
[35] S.D. Bass and P.V. Landshoff, Cavendish preprint HEP 94/4.
[36] F.E. Close and R.G. Roberts, Preprint RAL-94071 and F.E. Close, these proceedings.
[37] SMC Collaboration, J.P. Nassalski, these proceedings.
[38] T. Gehrmann and W.J. Stirling, Durham preprint DTP/94/38.
[39] E-665 FNAL Collaboration, H. Melanson, these proceedings.
[40] H1 Collaboration, V. Brisson, these proceedings.
[41] ZEUS Collaboration, M. Lancaster, these proceedings
[42] BCDMS Collaboration, A.C. Benvenuti *et al.*, Phys. Lett. **B223** (1989) 485.
[43] NMC Collaboration, P. Amaudruz *et al.*,Phys. Lett. **B295** (1992) 159.
[44] L.W. Whitlow *et al.*, Phys. Lett. **B282** (1992) 475.
[45] H1 Collaboration, I. Abt *et al.*, Nucl. Phys. **B407** (1993) 515.
[46] ZEUS Collaboration, M. Derrick *et al.*, Phys. Lett. **B316** (1993) 412.
[47] J. Feltesse, in Proc. HERA Workshop (DESY, 1987) p.33.
[48] D. Yu. Bardin *et al.*, Zeit. Phys. **C42** (1989) 679;
M. Böhm and H. Spiesberger, Nucl. Phys. **B294** (1987) 1081;
J. Blümlein , DESY preprint : DESY 94-044 ;
A. Akhundov *et al.*, CERN Preprint : CERN-TH.7339/94.
[49] S. Bentvelsen *et al.*, Proc. Workshop on Physics at HERA (DESY, 1991) p.23 ;
K.C. Hoeger, Proc. Workshop on Physics at HERA (DESY, 1991) p.43.
[50] A. Kwiatkowski, H. Spiesberger and H.J. Möring, Zeit. Phys. **C50** (1991) 165 Comput. Phys. Commun. **69** (1992) 155.
[51] A. Akhundov *et al.*, Proc. Workshop on Physics at HERA, vol 3, p.1285, DESY 1992.
[52] M. Glück, E. Reya and A. Vogt, Zeit. Phys. **C53** (1992) 127 and Phys. Lett. **B306** (1993) 391.
[53] V.N. Gribov and L.N. Lipatov, Sov.Journ.Nucl.Phys. **15** (1972) 438 and 675;
G.Altarelli and G.Parisi, Nucl.Phys. **B126** (1977) 298 ;
Yu.L.Dokshitzer, Sov.Phys.JETP **46** (1977) 641.
[54] K. Prytz, Phys. Lett. **B311** (1993) 286.
[55] H1 Collaboration, I. Abt *et al.*, Phys. Lett. **B321** (1994) 161.
[56] K. Golec-Biernat, Phys. Lett. **B328** (1994) 495.
[57] K. Prytz, Rutherford-Appleton Laboratory preprint : RAL-94-036.
[58] R.K. Ellis, Z. Kunszt and E.M. Levin, Fermilab preprint : Fermilab-PUB-93/350-T.
[59] A. Donnachie and P.V. Landshoff, Phys. Lett. **B332** (1994) 433.
[60] A. De Rujula *et al.*, Phys. Rev. D10 (1974) 1649.

[61] L.V. Gribov, E.M. Levin and M.G. Ryskin, Nucl. Phys. **B188** (1981) 555 and Phys. Rep. 100 (1983).
[62] R.D. Ball and S. Forte, CERN preprints CERN-TH.7265/94 and CERN-TH.7331/94.
[63] M. Virchaux, Invited talk to the Workshop 'QCD 20 years later' Aachen, 9-13 June 1992, Saclay Preprint DAPNIA/SPP 92-30.
[64] G. Raedel, these proceedings.
[65] E.A. Kuraev, L.N. Lipatov and V.S. Fadin, Phys.Lett. B60 (1975) 50 ;
Ya.Ya. Balitski and L.N. Lipatov, Sov.J.Nucl.Phys. **28** (1978) 822 and Zh.Eksperiment.I.Teor.Fiz. **72** (1977) 377.
[66] A. Donnachie and P.V. Landshoff, Phys. Lett. **B296** (1992) 227.
[67] J.R. Forshaw and P.N. Harriman, Phys. Rev. **D46** (1994) 3778;
R.E. Hancock and D.A. Ross, Nucl. Phys. **B383** (1992) 575;
J.Kwiecinski, A.D. Martin and P.J.Sutton, Phys. Rev. **D44** (1991) 2640 and Phys. Lett. **B264** (1991) 199;
J.C. Collins and P.V. Landshoff, Phys. Lett. **B276** (1992) 196;
A. Capella *et al.*, Phys. Lett. **B337** (1994) 358;
R. Peschanski and S. Wallon, Saclay preprint : SPhT 94/90.
[68] A.H. Mueller, Nucl. Phys. **B415** (1994) 373.
[69] J. Bartels, K. Charchula and J. Feltesse, Proc. Workshop on Physics at HERA (DESY, 1991) p.193.
[70] A.J.Askew *et al.*, Phys. Lett. **B325** (1994) 212; Phys. Rev. **D49** (1994) 4402.
[71] K. Golec-Biernat, M.W. Krasny and S. Riess, DESY preprint : DESY 94-131.
[72] E.M. Levin *et al.*, Nucl. Phys. **B357** (1991) 167.
[73] M. Bengtsson, G. Ingelman and T. Sjöstrand, Nucl. Phys. **B301** (1988) 554.
[74] L. Lönnblad, Comput. Phys. Comm. **71** (1992) 15.
[75] L. Lönnblad, CERN preprint : CERN-TH.7307/94.
[76] H1 Collaboration, I. Abt *et al.*, DESY 94-033, submitted to Z. Phys. C.
[77] K. Golec-Biernat *et al.*, Phys. Lett. **B335** (1994) 220.
[78] A.H. Mueller, Nucl. Phys. B (Proc. Suppl.) **18C** (1990) 125 and J.Phys. G17 (1991) 1443.
[79] A.J. Askew *et al.*, CERN preprint : CERN-TH.7357/94.
[80] A.H. Mueller Nucl. Phys. **B282** (1987) 727.
[81] V. Del Duca and C.R. Schmidt,Phys. Rev. **D49** (1994) 4510 and DESY preprint : 94-114.
[82] W.J. Stirling, Durham preprint : DTP/94/04 ; and Phys. Lett. **B329** (1994) 386.
[83] M.G.Ryskin and M.Besançon, Proc. Workshop on Physics at HERA (DESY, 1991) p.215, and references therein.
[84] ZEUS Collaboration, M. Derrick *et al.*, Phys. Lett. **B315** (1993) 481.
[85] H1 Collaboration, J. B. Dainton, "Results from the H1 Experiment at HERA.", in Proc. XVI International Symposium on Lepton Photon Interactions, Cornell, Ithaca, USA, August 1993, A. De Roeck, "Results from the H1 Experiment.", to appear in Proc. of the Europhysics Conf. on HEP, Marseille, France, July 1993. DESY preprint : DESY 94-005 (1994).
[86] G.A. Schuller and H. Spiesberger, Proc. Workshop on Physics at HERA (DESY, 1991) p.1419 and references therein.
[87] G. Ingelman and P. Schlein, Phys. Lett. **B152** (1985) 256.
[88] UA8 Collaboration, A. Brandt *et al.*, Phys. Lett. **B297** (1992) 417.
[89] P. Bruni and G. Ingelman, DESY preprint : DESY 93-187 and Proc. of the Europhysics Conf. on HEP, Marseille 1993, 595.
[90] H. Jung, DESY preprint : DESY 93-182.
[91] N.N. Nikolaev and B.G. Zakharov, Zeit. Phys. C53 (1992) 331.
[92] H1 Collaboration, T. Ahmed *et al.*, Nucl. Phys. **B429** (1994) 477 and DESY preprint : DESY 94-133.
[93] G. Ingelman and K. Prytz, Zeit. Phys. **C58** (1993) 285.
[94] ZEUS Collaboration, M. Derrick *et al.*, DESY preprint : DESY 94-117.
[95] ZEUS Collaboration, F. Barreiro, these proceedings.
[96] NMC Collaboration, A. Sandacz, paper gls0267 submitted to this conference.
[97] EMC Collaboration, J.J. Aubert *et al.*, Phys. Lett. **B161** (1985) 203 and J. Ashman *et al.*, Zeit. Phys. **C39** (1988) 169.
[98] NMC Collaboration, P. Amaudruz *et al.*, Zeit. Phys. **C54** (1992) 239.
[99] ZEUS Collaboration, M. Derrick *et al.*, Phys. Lett. **B332** (1994) 228.
[100] CDF Collaboration, T. Devlin, paper gls0413 submitted to this conference.
[101] D0 Collaboration, A. Brandt, these proceedings.
[102] J.D. Bjorken, Phys. Rev. **D47** (1993) 101.

Discussion

M. Islam, University of Connecticut:
The fact that there are a number of models to explain the behaviour of $F_2(x,Q^2)$ in the small x region shows that we do not adequately understand the non-perturbative effects in these soft interactions. Can you comment?
J. Feltesse:
The hard mechanisms which are in competition at low x are based on perturbative QCD. The hope is that the understanding of the dynamics at low x will provide a bridge to the unknown non perturbative domain.
D. Schildknecht, Bielfeld:
A long time ago, it was suggested that deep inelastic scattering at small x was caused by diffractive high-mass contributions to the imaginary part of the forward virtual Compton amplitude. As a consequence of this picture of Generalised Vector Dominance, shadowing in DIS on complex nuclei was predicted and also diffractive production of high-mass vector states. Well, shadowing in DIS was finally revealed a few years back, and diffractive production of high-mass states is now observed at HERA; so qualitatively this picture is correct. Quantitatively, in this picture F_2 is connected with diffractive production by a sum rule which is experimentally testable. Thus, while the large rapidity gap events do not *directly* explain the rise of F_2 at small x, they may do so indirectly; i.e. in the same way as the total real photoproduction cross section is related to forward ρ,ω,ϕ production.
J. Feltesse:
We do see in the data rapidity gap events with a large invariant mass M_X and that part of the diffractive deep inelastic events is due to production of vector mesons. The assumption that the Generalised Vector Dominance Model can describe the rise of F_2 and the diffractive events has to be confronted with the data.
P. Schlein, UCLA:
In your exclusive final state ρp events, the proton is not observed . How sure are you that the proton is alone, i.e. that it is not accompanied by some unobserved low mass system?
J. Feltesse:
We are not sure that in DIS exclusive vector meson events the proton is alone in the beam pipe. The H1 collaboration, using his forward tagging detectors, finds that about 30% of diffractive events with $\eta_{max} < 1.8$ involve diffractive dissociation of the proton. By Monte Carlo studies the ZEUS collaboration finds that the proton dissociates in 15% of the ρ production deep inelastic events.

To remove non-exclusive background in the main detector, the ZEUS analysis requires $E_{\pi+\pi-}/P_{\pi+\pi-} < 1.5$, where $E_{\pi+\pi-}$ is the calorimeter energy excluding the scattered electron and $P_{\pi+\pi-}$ is the sum of momenta of the two oppositely charged tracks. The H1 analysis of the exclusive VM candidates explicitely excludes the events with more than 1.5 GeV of energy deposited in the calorimeters not associated to the two oppositely charged particles or to the scattered electron. So, we do have events where there are more than the two tracks of the ρ. We will investigate these events with the high statistics accumulated in 1994.